



ORIGINAL ARTICLE

Design, synthesis, cytotoxicity and 3D-QSAR analysis of new 3,6-disubstituted-1,2,4,5-tetrazine derivatives as potential antitumor agents



Álvaro Cañete-Molina^a, Christian Espinosa-Bustos^a, Marcos González-Castro^a, Mario Faúndez^b, Jaime Mella^c, Ricardo A. Tapia^a, Alan R. Cabrera^{a,d}, Iván Brito^e, Adam Aguirre^b, Cristian O. Salas^{a,*}

^a Departamento de Química Orgánica, Facultad de Química, Pontificia Universidad Católica de Chile, 702843 Santiago de Chile, Chile

^b Departamento de Farmacia, Facultad de Química, Pontificia Universidad Católica de Chile, 702843 Santiago de Chile, Chile

^c Instituto de Química y Bioquímica, Facultad de Ciencias, Universidad de Valparaíso, 2360102, Av. Gran Bretaña 1111, Playa Ancha, Valparaíso, Casilla 5030, Chile

^d Universidad Bernardo O'Higgins, Departamento de Ciencias Químicas y Biológicas, Laboratorio de Bionanotecnología, General Gana 1702, Santiago, Chile

^e Departamento de Química, Facultad de Ciencias Básicas, Universidad de Antofagasta, Av. Angamos 601, Antofagasta, Chile

Received 3 November 2016; accepted 1 April 2017

Available online 9 April 2017

KEYWORDS

Tetrazine derivatives;
Anticancer activity;
Apoptosis;
3D-QSAR

Abstract We synthesized two new series of 3-substituted-6-(2,5-dimethylpyrazol-1-yl)-1,2,4,5-tetrazines and analysed them for a potential role as antitumor agents. Twenty-two compounds were obtained, and four molecular structures were determined by X-ray diffraction analysis. Using flow cytometry and MTT assay, potential action on cell toxicity was determined for each of the compounds for four cancer cell lines. The potency and selectivity demonstrated by these compounds are dependent on the cancer cell line, where the following compounds were found the most promising agents against certain cell lines: compounds **1i** and **1j** for HL-60 cells, **1a** and **1b** on HCT116 cells, **1f** on Hela cells and **2h** on H1975 cells. The action exerted by these compounds is comparable to the well-known cancer treatment drug etoposide and higher than vatalanib. To arrive at the structural requirements for activity on each cell line, a SAR and 3D-QSAR analysis was carried out. From the 3D-QSAR models, steric and electronic features were identified in the aromatic

* Corresponding author.

E-mail address: cosalas@uc.cl (C.O. Salas).

Peer review under responsibility of King Saud University.



Production and hosting by Elsevier

<http://dx.doi.org/10.1016/j.arabjc.2017.04.002>

1878-5352 © 2017 The Authors. Production and hosting by Elsevier B.V. on behalf of King Saud University.

This is an open access article under the CC BY-NC-ND license (<http://creativecommons.org/licenses/by-nc-nd/4.0/>).

centres, and were key components for cytotoxic activity on HL-60 cell lines. The cytometry results suggest that some tetrazine derivatives induce apoptosis on HCT116 cells.

© 2017 The Authors. Production and hosting by Elsevier B.V. on behalf of King Saud University. This is an open access article under the CC BY-NC-ND license (<http://creativecommons.org/licenses/by-nc-nd/4.0/>).

1. Introduction

Cancer is one of the most important problems in public health, and is the main disease responsible for deaths worldwide (Siegel et al., 2013). Currently cancer Chemotherapy represents a constant, global and interdisciplinary research effort because it is an urgent need to promote and extend the quality of life for the world population. New antitumor therapies point towards new compounds that demonstrate selective anticancer actions, and thus must exhibit a cytotoxic effect on malignant cells, without damaging normal cells (Chan et al., 2016; Rani and Kumar, 2016; Dörsam and Fahrer, 2016; Ni et al., 2015a, 2015b).

Most of the known synthetic anticancer drugs are heterocyclic compounds, and several of them correspond to nitrogen heterocycles (Sherer and Snape, 2015; Dolezal and Zitko, 2015; Shiro et al., 2015; Khan et al., 2014). In the last decades, a large number of phthalazine derivatives have been synthesized and their antitumor activity has been reported, emerging as a promising and attractive scaffold (Abouzeid et al., 2012; Bold et al., 2000; Eldehna et al., 2015; Zhang et al., 2010). Among them, a 1,4-disubstituted phthalazine vascular endothelial growth factor receptor (VEGFR) inhibitor, called vatalanib (PTK-787, Fig. 1), is currently in phase II in patients with advanced and

metastatic pancreatic adenocarcinoma after first-line gemcitabine therapy (Dragovich et al., 2014). In another study, 1-piperazinyl phthalazine derivative **I** (Fig. 1), inhibited VEGFR-2 at sub-micromolar IC₅₀ values and also exhibited potent activity in a broad spectrum cancer cell lines (Abou-Seri et al., 2016). A compound called LY-2940680 (Fig. 1), was developed as a potential anticancer agent targeting the Hedgehog (Hh) pathway, which is involved in several cancers (Banerju and Hadden, 2014; Xin, 2015; Ruch and Kim, 2013). LY2940680, a phthalazine-based small molecule developed by Eli Lilly & Co., is a potent Hh inhibitor with potential anticancer activity in a medulloblastoma (MB) cell line (Wilson et al., 2013) and has also shown to be effective in an orally-administered murine model of Hh-dependent MB. This compound is currently undergoing Phase I and II clinical trials in order to confirm its effectiveness against different human cancers (Bender et al., 2011).

Another Hh signalling pathway inhibitor developed by Novartis related to LY2940680, NVP-LEQ506 (Fig. 1) (Peukert et al., 2013; Miller-Moslin et al., 2009), is considered as a prominent anticancer agent, and is now in phase I of clinical trials. NVP-LEQ506, a 4-benzylpyridazine derivative, was shown to reduce Gli mRNA expression and promote tumour regression in a murine allograft of Hh-dependent MB.

Two of the just mentioned compound (**I** and NVP-LEQ506), in addition to the phthalazine or pyridazine ring, have a piperazinyl group, a small and rigid heterocyclic backbone, which has been an attractive pharmacological scaffold present in several other antitumor drugs (Patel and Park, 2013).

Therefore, considering the anticancer activity and the chemical structures of compounds shown in Fig. 1, we designed a series of 3-substituted-6-(2,5-dimethylpyrazol-1-yl)-1,2,4,5-tetrazines (**1a-l** and **2a-j**, Fig. 1), with the goal of developing new drug-like compounds as active anticancer agents with respect to the source compounds. In our design, we used the mixture of two well-known methodologies in medicinal chemistry with the proposal of discovering and optimizing biologically active compounds. One of these strategies corresponded to fragment-based drug design (Lanning et al., 2016; Wang et al., 2016; McBride et al., 2016; Liao et al., 2011). This approach combines fragments of the active molecules or pharmacophores with a specific linker, where these moieties are prominent structural motifs. The other strategy was bioisosterism (Moreira-Lima and Barreiro, 2005; Meanwell, 2011), which is a special process of molecular modification of a lead compound that changes some features of this compound, such as size, shape, electronic distribution, polarizability, dipole, polarity, lipophilicity, and pKa. In the new compounds, we replaced the phthalazine moiety or the pyridazine ring for the isosteric tetrazine ring, while the piperidinyl-benzamide (in blue dash square for series **I**, **1a-l**), the piperazinyl-phenyl moiety (in blue dash square for series **II**, **2a-j**) and the pyrazole ring (in red dash square) were maintained in both series. For the compound **2e**, piperazinyl-phenyl portion was replaced by piperidinyl-phenyl moiety. It is noteworthy that although the incorporation of tetrazine rings has been recently considered in the development of antitumor compounds (Xu et al., 2016), this heterocyclic system already has been used successfully to develop compounds with biomedical applications (Devaraj et al., 2008; Devaraj and Weissleder, 2011; Wu et al., 2014; Ni et al., 2015a, 2015b).

Therefore, in the present work, we report the design and synthesis of twenty-two new tetrazine derivatives and carried out an *in vitro* study of their cytotoxic activity against four cancer cell lines (H1975, HL-60, HCT116 and HeLa) and VERO cells to determine potential antitumor effects as well as the selectivity. Additionally, the ability

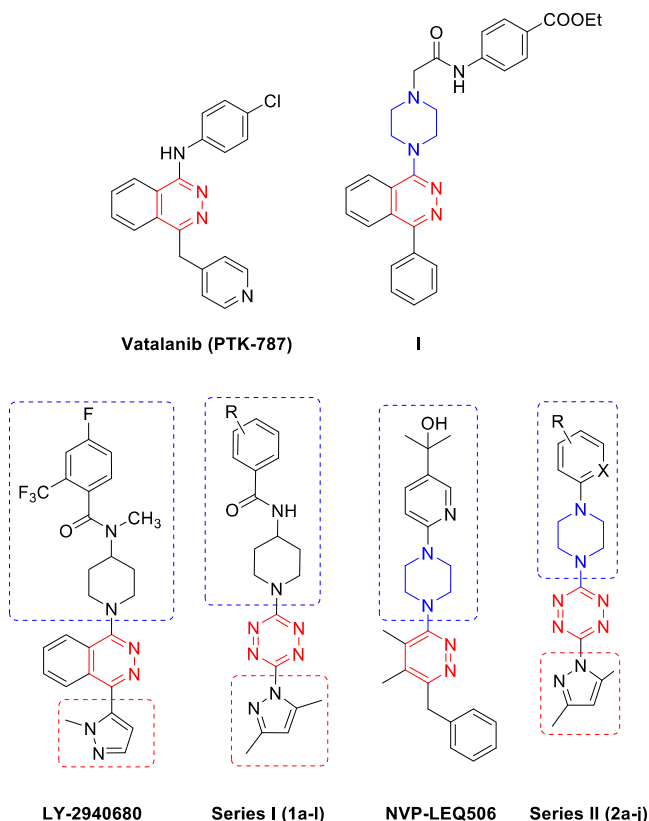
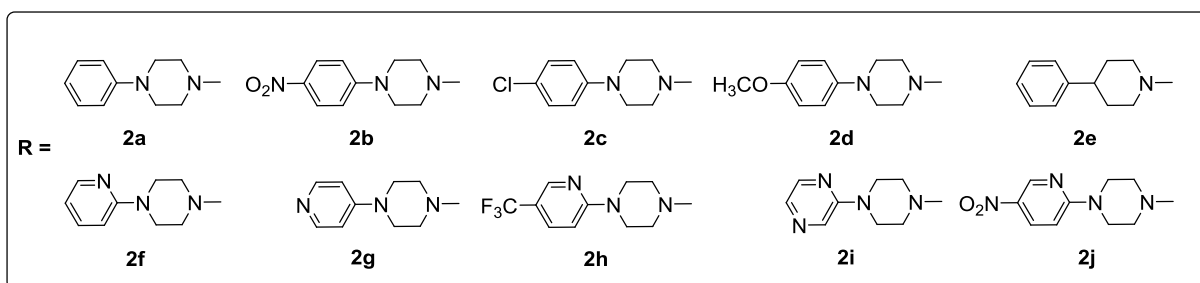
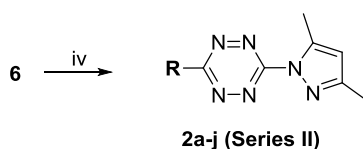
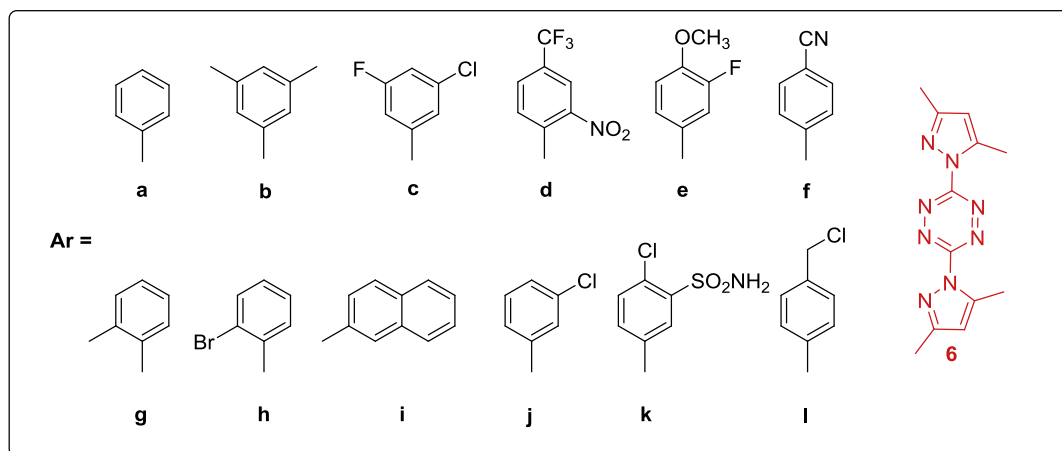
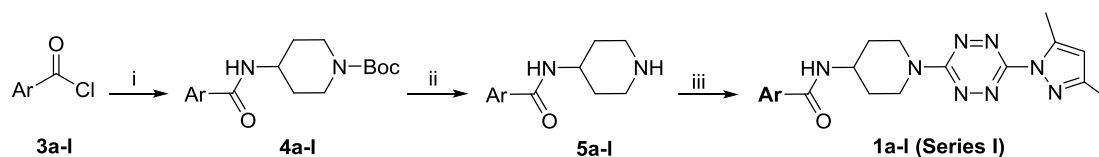


Fig. 1 Chemical structures of phthalazine and pyridazine derivatives with anticancer activity and the target compounds **1a-l** and **2a-j**. In blue and red dashed squares, appear fragments of the reference compounds that were considered in the design of new tetrazine derivatives for both series.



Scheme 1 Reagents and conditions: (i) *tert*-Butyl-4-aminopiperidine-1-carboxylate, THF/CH₂Cl₂, rt, 12 h, 65–83%; (ii) TFA, rt, 30 min; (iii) **6**, TEA (excess), acetonitrile, rt, overnight, 30–69%; (iv) Arylpiperazines or arylpiperidines, TEA (excess), acetonitrile, rt, overnight, 52–84%.

to induce apoptosis as a possible action mechanism of these compounds, was done by flow cytometry for all the studied cancer cell lines.

Finally, we used comparative molecular field analysis (CoMFA) and comparative molecular similarity indices analysis (CoMSIA), and we developed a 3D-QSAR model, with the aim of analysing the *in vitro* cytotoxic activity of all the compounds under study.

2. Results and discussion

2.1. Chemistry

Synthesis of these tetrazine derivatives from both series was achieved according to [Scheme 1](#), using tetrazine **6** ([Coburn et al., 1991](#)), as the starting material, and simple well-known organic reactions at room temperature. To obtain compounds

from **series I (1a-l)**, phenyl-piperazine derivatives **5a-l** were prepared from corresponding aryl chloride **3a-l**. Nucleophilic substitution of **3a-l** by *tert*-butyl-4-aminopiperidine-1-carboxylate, in a mixture of THF and CH₂Cl₂ (1:1), furnished Boc-derivatives **4a-l** (65–83%). Deprotection reactions from these Boc-derivatives were carried out with trifluoroacetic acid (TFA), yielding the free-amines **5a-l**. Without further purification, these free-amines were reacted with **6** in acetonitrile as a solvent, and in the presence of triethylamine (TEA), yielded target compounds **1a-l** (40–69%) ([Rusinov et al., 2006](#)). Such low yields in the last step could be related to the work-up and cleansing stages (including chromatographic separations). Similarly, compounds belonging to **series II (2a-j)** were synthesized through the nucleophilic substitution of **6** by commercially available aryl-piperazines in acetonitrile as solvent with TEA present. Yields from this step were higher than the other

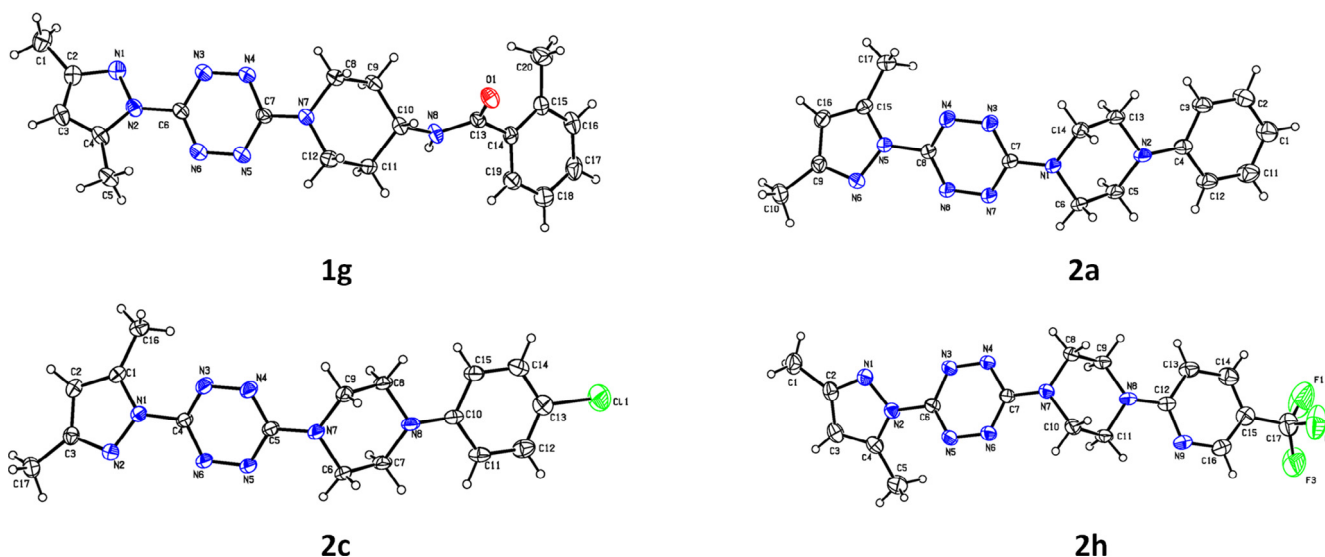


Fig. 2 Molecular structure of selected tetrazines **1g**, **2a**, **2c** and **2h**. Thermal ellipsoids are shown with 30% probability.

analogues (52–84%), probably due to the purity and stability of the nucleophiles. Target compound chemical structures from both series were established by their spectral properties (IR, ^1H NMR, ^{13}C NMR and HRMS, see Section 4 and [Electronic supplementary information, ESI](#)) and for compounds **1g**, **2a**, **2c** and **2h**, by X-ray crystal structure analysis.

2.2. Crystallographic studies

Molecular structures from the four selected tetrazine derivatives **1g**, **2a**, **2c** and **2h** were determined by X-ray crystallography (Fig. 2). Selected distances, angles and dihedral angles are summarized in [Table S-1](#) (see [Electronic supplementary information](#)). All four tetrazines had similar molecular structure. Bond distances and angles were in the typical range of similar organic systems (Patra et al., 2004). Tetrazines exhibit a bending point in the piperazine ring with dihedral angles of $-111.1(3)^\circ$ (C7-N7-C8-C9, for tetrazine **1g**), $-116.3(2)^\circ$ (C7-N1-C14-C13, for tetrazine **2a**), $-125.6(0)^\circ$ (C5-N7-C6-C7, for tetrazine **2c**) and $-103.8(3)^\circ$ (C7-N7-C10-C11, for tetrazine **2h**), due to the chair shape adopted by the piperazine portion of the molecule. The pyrazole group is rotated slightly out of the plane of the tetrazine ring, showing dihedral angles of $24.0(4)^\circ$ (N1-N2-C6-N3, for tetrazine **1g**), $32.5(2)^\circ$ (N6-N5-C8-N8, for tetrazine **2a**), $28.6(7)^\circ$ (N2-N1-C4-N6, to the tetrazine **2c**) and $33.2(3)^\circ$ (N1-N2-C6-N3, for tetrazine **2h**). Tetrazine **1g** exhibits a rotation out of the plane of the carbonyl group with respect to phenyl ring ($-49.5(4)^\circ$ (C15-C14-C13-O1)) and in the tetrazine **2h** a coplanarity is shown between the piperazine and the pyridine group ($11.4(3)^\circ$ C11-N8-C12-N9)).

2.3. Cytotoxic studies

We studied the *in vitro* cytotoxic effect of the previously mentioned compounds on H1975, HL-60, HCT116 and HeLa cancer cell lines and non-neoplastic Vero cells. Conventional colorimetric assay was used to estimate the IC_{50} values, representing the concentration of a drug that is needed for 50% inhibition *in vitro* after 72 h of continuous exposure to

compounds. Triplicate tests using four serial dilutions (from 0.05 to 50 μM) were done for each sample, using the drugs etoposide and vatalanib as a positive control.

[Table 1](#) shows the IC_{50} cytotoxicity values for compounds **1a-l**, **2a-j** and **6**. In general, tetrazine derivatives showed to be heterogeneous, but in the most cases the unsymmetrical tetrazines were more potent than the symmetrical starting material (**6**, with IC_{50} values on all cancer cell lines $> 50 \mu\text{M}$). In a general analysis of cytotoxicity, HCT116 cells seemed to be more resistant (all compounds tested with IC_{50} value $> 5 \mu\text{M}$). H1975, HL60, HeLa and Vero cells had variable sensitivity. However, after further cytotoxicity analysis for each cancer cell line, we conclude that:

- (i) For HCT116 cells, all compounds were less active than etoposide. On the contrary, compounds **1b**, **1c**, **1h**, **1i**, **1j** and **1l** showed higher activity than vatalanib. All derivatives were less selective than etoposide and more selective than vatalanib (SI value = 0.3).
- (ii) For HeLa cells, compounds **1f** and **1h** (IC_{50} values = 6.6 and 4.1 μM , respectively) were more potent than etoposide, and exhibited better or equal selectivity than the same reference compound (SI values = 7.6 and 3.2). In addition, compounds **1b**, **1c** and **1j** showed similar activity, but a higher selectivity compared to etoposide (SI values = 5.9, 5.4, and 7.6, except **1j** with a SI value < 3.0). It is important to mention that all active compounds (IC_{50} values $< 11 \mu\text{M}$) were more potent and selective than vatalanib.
- (iii) For HL60 cells, these were our best results in potency and selectivity from some of the tetrazine derivatives compared to etoposide and vatalanib. Specifically, compounds **1h-l** elicited the lowest IC_{50} values in this study ($< 1.9 \mu\text{M}$). Interestingly, **1i** and **1j** were five to six times more selective than etoposide and more than one hundred times more selective than vatalanib (SI values = 27 and 19). **1i** and **1j** are the most promising compounds for further biological studies.

Table 1 *In vitro* cytotoxicity of compounds **1a-1l**, **2a-2j** and **6**, on cancer cell lines and Vero cells.

Compound	IC ₅₀ values in (μM) ^a								
	HCT116 ^b	SI ^c	HeLa ^d	SI	HL-60 ^e	SI	H1975 ^f	SI	VERO ^g
1a	> 50	–	> 50	–	> 50	–	14 ± 2.5	0.5	7.3 ± 1.3
1b	7.7 ± 0.3	6.5	8.5 ± 1.0	5.9	> 50	–	> 50	–	> 50
1c	6.9 ± 0.8	7.2	9.2 ± 2.5	5.4	> 50	–	> 50	–	> 50
1d	> 50	–	> 50	–	> 50	–	> 50	–	> 50
1e	> 50	–	> 50	–	> 50	–	> 50	–	28 ± 4.9
1f	> 50	–	6.6 ± 1.0	7.6	> 50	–	> 50	–	> 50
1g	> 50	–	> 50	–	> 50	–	> 50	–	> 50
1h	5.4 ± 1.3	2.4	4.1 ± 1.9	3.2	1.9 ± 1.3	6.8	> 50	–	13 ± 3.2
1i	8.6 ± 4.2	2.8	> 50	–	0.9 ± 0.5	27	20 ± 8.2	1.2	24 ± 1.2
1j	5.4 ± 0.9	2.4	8.3 ± 4.0	1.6	0.7 ± 0.02	19	8.7 ± 4.6	1.5	13 ± 3.1
1k	23 ± 6.1	–	> 50	–	0.5 ± 0.05	4.4	2.4 ± 0.6	0.9	2.2 ± 1.4
1l	11 ± 3.1	0.7	11 ± 2.8	0.7	1.8 ± 1.0	4.3	4.4 ± 1.0	1.8	7.7 ± 0.5
2a	> 50	–	> 50	–	43 ± 0.8	–	> 50	–	> 50
2b	> 50	–	> 50	–	> 50	–	> 50	–	> 50
2c	> 50	–	> 50	–	> 50	–	> 50	–	> 50
2d	> 50	–	> 50	–	43 ± 0.6	–	> 50	–	> 50
2e	> 50	–	32 ± 0.7	1.6	31 ± 0.8	1.6	> 50	–	> 50
2f	45 ± 0.8	1.1	23 ± 0.7	2.2	23 ± 0.6	2.2	> 50	–	> 50
2g	> 50	–	32 ± 0.9	1.6	8.1 ± 0.8	6.2	> 50	–	> 50
2h	> 50	–	> 50	–	29 ± 0.7	1.7	7.4 ± 0.6	6.8	> 50
2i	> 50	–	> 50	–	46 ± 0.7	–	> 50	–	> 50
2j	> 50	–	> 50	–	47 ± 0.5	–	> 50	–	> 50
6	> 50	–	> 50	–	> 50	–	> 50	–	> 50
Etoposide	2.8 ± 0.2	8.9	8.2 ± 0.3	3.0	6.2 ± 0.2	4.0	8.0 ± 0.3	3.1	> 25 ^h
Vatalanib	18 ± 5.3	0.3	16 ± 3.9	0.3	31 ± 4.3	0.1	37 ± 6.0	0.1	4.5 ± 0.1

^a IC₅₀ values were determined in three independent experiments for triplicate in the range of 0.05–50 μM. The best values of cytotoxicity are in bold font.

^b Human colorectal carcinoma cells.

^c Selectivity index (SI) = IC₅₀ values of pure compound in a normal cell line/IC₅₀ values of the same pure compound in cancer cell line (In some cases where the IC₅₀ values on Vero cells was > 50 μM, the SI value was calculated considering that this is = 50 μM).

^d Human cervix adenocarcinoma cells.

^e Human promyelocytic leukaemia cells.

^f Human lung cancer cells.

^g Green monkey normal kidney cells.

^h At > 25 μM this compound decreased its solubility in the cell cultures.

(iv) For H1975 cells, compounds **1k**, **1l** and **2h** exhibited from higher to similar potency than etoposide (IC₅₀ values = 2.4, 4.4 and 7.4 μM, respectively), but only **2h** showed a higher selectivity (SI value = 6.8). Moreover, compounds **1a**, **1i**, **1j**, **1k**, **1l** and **2h** were more potent and selective than vatalanib (IC₅₀ values < 20 μM and SI values > 0.5).

On the other hand, antitumor drugs should exhibit low toxicity in mammalian host cells, and thus, more selective compounds are very promising for the development of new antitumor agents. These results are in agreement with the National Cancer Institute (NCI) protocols, which consider active compounds exhibiting IC₅₀ values < 10 μM or 15 μM (NCI/NIH, 2014).

2.4. Structure activity relationship (SAR)

The SAR analysis depends on the comparison between the cytotoxic activity against cancer cell lines and structural variations from compounds of the **series I** or **II**. Thus, a look at the

IC₅₀ values for each cancer cell line suggests that from a chemical point of view, there are interesting structural features worth considering.

Firstly, in general, compounds from **series I** were more potent than **series II**. This evidence could indicate, that amide moiety in the compounds of **series I**, is an important linker between the aromatic ring and the heterocyclic system, and is the major structural difference with the compounds from the **series II**.

Secondly, some substitutions on the phenyl moiety of **1a**, led us to understand the scope of some chemical modifications. This was especially notable in some cases where there existed a clear behaviour on the four cancer cell lines. For example, when the benzene ring was substituted in *ortho*-position with an electron-donating group (methyl for **1g**, IC₅₀ values > 50 μM), this modification did not generate an increase in the cytotoxic activity on four cancer cell lines. However, if this substituent was a bromine atom (**1h**), the cytotoxicity increased significantly (IC₅₀ values < 5 μM), except on H1975 cells. On the other hand, a 2,4-disubstitution (**1d**, IC₅₀ values > 50 μM) was unsuccessful at obtaining a

compound with better activity compared with **1a**. Regarding compounds with substitution on *meta*-positions, **1j** exhibited a significant improvement in potency against all cell panels (IC_{50} values = 0.7–13 μ M). Nevertheless, in the compounds that have a 3,4- or 3,5-disubstitution pattern (**1e** or **1k** and **1b** or **1c**, respectively), the effect on the cytotoxicity depends on the combination of the stereoelectronic features of these groups. A similar behaviour was observed for the *para*-substitution, and this is because when an electron-withdrawing group was incorporated (cyano group in **1f**), the cytotoxic activity did not change compared to **1a**, except in HeLa cells. However, when substitution was done by a chloromethyl group (**1l**), diminished IC_{50} values were observed in all cell panels (< 11 μ M).

In a third observation, when comparing **1a** with **1i**, the IC_{50} values indicated that replacement of the benzene ring by a naphthalene ring was relevant for an increase in cytotoxicity against HCT116 cells and very significant on HeLa cells. On H1975 cells, this modification slightly enhanced cytotoxicity, and on HL-60 cells, it was unsuccessful.

For the less active tetrazine derivatives in this study (**series II**), the influence of the substituents in the phenyl group, on the increase in cytotoxicity, was not achieved when reference compound **2a** was modified. Only two compounds exhibited a significant potency and selectivity; **2g** on HL-60 cells and **2h** on H1975 cells (IC_{50} values of 8.1 and 7.4 μ M, and SI values of 6.2 and 6.8, respectively). These results indicate that, on HL-60 cell, the addition of an extra nitrogen atom and their position in the aromatic ring, increased the cytotoxic activity (**2f-h**, IC_{50} values < 29 μ M). But, if in this heterocyclic moiety, an electron-withdrawing group or an extra nitrogen atom is incorporated, the cytotoxicity is reduced (**2h-j**, IC_{50} values > 29 μ M).

Finally, the SAR analysis mentioned above, provides information about the effectivity of chemical modification for these tetrazine derivatives on the cytotoxic activity in cancer cell lines. Furthermore, 3D-QSAR gives an even more precise explanation of the cytotoxicity differences of the studied compounds. These separate 3D-QSAR results and discussions are given in the following section.

2.5. 3D-QSAR

From the works of Cramer and Klebe (Cramer et al., 1988; Klebe et al., 1994), comparative molecular field analysis (CoMFA) and comparative molecular similarity indices analysis (CoMSIA) are useful methodologies to understand the pharmacological properties of a series of compounds. The steric and electrostatic maps obtained help to (a) understand the nature of ligand-receptor interactions; (b) predict biological affinity and (c) aid in the rational design of new promising compounds. 3D-QSAR studies were performed on the four cancer cell lines with compounds that had IC_{50} values < 50 μ M. Information related to steric (S), electrostatic (E) and hydrophobic (H) properties was concordant among the models. In the CoMSIA studies, the donor and acceptor fields were not related to the observed activity. Models exhibited good $r^2 > 0.8$, small standard error of estimation analysis (SEE) of non-cross-validation, as well as high F -test values (F). 3D-QSAR analysis, from the results of the cytotoxicity in HL60 cells gave the most extensive information about the chemical requirements of tetrazine derivatives. In Table 2, we report the step-by-step search to find the best CoMFA and CoMSIA field combinations in the HL60 model. The criterion to select the best models was the LOO cross validated r^2 (q^2). Compounds exhibited a good linear correlation between their actual versus predicted pIC_{50} , for both CoMFA and CoMSIA models (Fig. 3), and the residual value was less than 0.25. The experimental versus calculated biological activity is shown in Table 3.

CoMFA and CoMSIA contour maps for HL60, HCT116 and H1975 shows a large green polyhedron around the aromatic ring at the end of the most active compounds, and a yellow polyhedron around the piperazine and piperidine in the less active compounds (Fig. 4(A, B), 5(A, B), S1 (A, B) and S3 (A)). This suggests that bulky groups such as sulphonamide in compound **1k**, are highly favourable for antitumor activity. In fact, the most active compounds usually carry halogens or a bulky naphthalene ring at the end. According to the HL60 Models, the best positions for inserting bulky groups should be positions 3, 4 and 5 of the benzene ring. However, the presence of

Table 2 Search of the best CoMFA and CoMSIA models using several field combinations.^a

Model	q^2	N	SEP	SEE	r^2	F	Field contributions ^b		
							S	E	H
CoMFA-S	0.729	3	0.477	0.085	0.979	288.321	1		
CoMFA-E	0.539	2	0.563	0.332	0.321	25.625		1	
CoMFA-SE	0.777	4	0.423	0.102	0.989	287.325	0.602	0.398	
CoMSIA-S	0.73	2	0.456	0.256	0.921	77.523	1		
CoMSIA-E	0.54	4	0.665	0.161	0.932	72.121		1	
CoMSIA-H	0.79	1	0.396	0.322	0.889	95.35			1
CoMSIA-SE	0.813	4	0.37	0.152	0.978	112.113	0.414	0.586	
CoMSIA-SEH	0.743	1	0.422	0.255	0.905	110.289	0.185	0.371	0.444
CoMSIA-SH	0.756	1	0.366	0.266	0.902	114.102	0.303		0.697
CoMSIA-EH	0.671	1	0.421	0.361	0.877	73.246		0.459	0.541

^a q^2 = Square of the LOO cross-validation (CV) coefficient; N = Optimum number of components; SEP = Standard error of prediction; SEE = Standard error of estimation of non-CV analysis; r^2 = Square of the non-CV coefficient; F is the F -test value. S, E and H are the steric, electrostatic and hydrophobic contributions respectively. The best values of q^2 are in bold font.

^b The hydrogen bond donor and hydrogen bond acceptor fields did not correlate with activity.

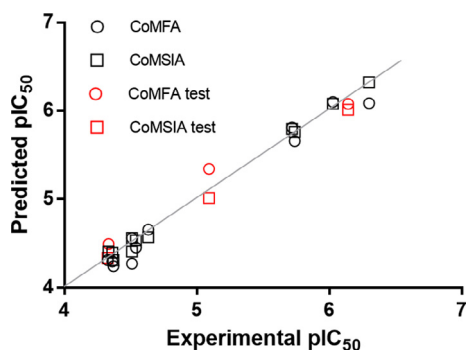


Fig. 3 CoMFA and CoMSIA experimental versus predicted pIC_{50} applied to tetrazine derivative cytotoxicity on HL60 cells.

groups such as halogens or methyl in the compounds **1b-c**, **e-f**, implicates that a higher steric hindrance is necessary in these positions. Use of other non-planar bulky rings such as adamantyl ring, would be interesting to explore too. The less active compounds do not have the amide linker between piperidine or piperazine and the phenyl ring, and these molecules point their terminal rings to the yellow polyhedron. So, lengthening of the chains is beneficial for activity. CoMSIA Hydrophobic contour maps (Figs. 5(E, F), S1 and S2(E,F)) complement that, the hydrophobic favourable yellow polyhedra are around the halogens and phenyls in the most active derivatives. Only the contour maps in H1975 (Fig. S3(B)) show a predominance of hydrophilic polyhedra around the terminal ring of the

Table 3 Experimental versus predicted activity for CoMFA and CoMSIA models for HL60 cells.

Compound	Experimental pIC_{50} (M)	CoMFA		CoMSIA	
		Predicted pIC_{50} (M)	Residual	Predicted pIC_{50} (M)	Residual
1h	5.7190	5.8120	-0.09	5.7950	-0.08
1i	6.0269	6.1020	-0.08	6.0810	-0.05
1j^a	6.1427	6.0800	0.06	6.0130	0.13
1k	6.3010	6.0870	0.21	6.3230	-0.02
1l	5.7399	5.6600	0.08	5.7630	-0.02
2a	4.3709	4.2430	0.13	4.3120	0.06
2d	4.3625	4.2960	0.07	4.3930	-0.03
2e	4.5102	4.5620	-0.05	4.5620	-0.05
2f	4.6349	4.6570	-0.02	4.5720	0.06
2g^a	5.0931	5.3440	-0.25	5.0150	0.08
2h	4.5411	4.4540	0.09	4.5340	0.01
2i^a	4.3336	4.4940	-0.16	4.4050	-0.07
2j	4.3274	4.3120	0.02	4.3350	-0.01
Vatalanib	4.5102	4.2702	0.24	4.4052	0.11

^a Test set compounds.

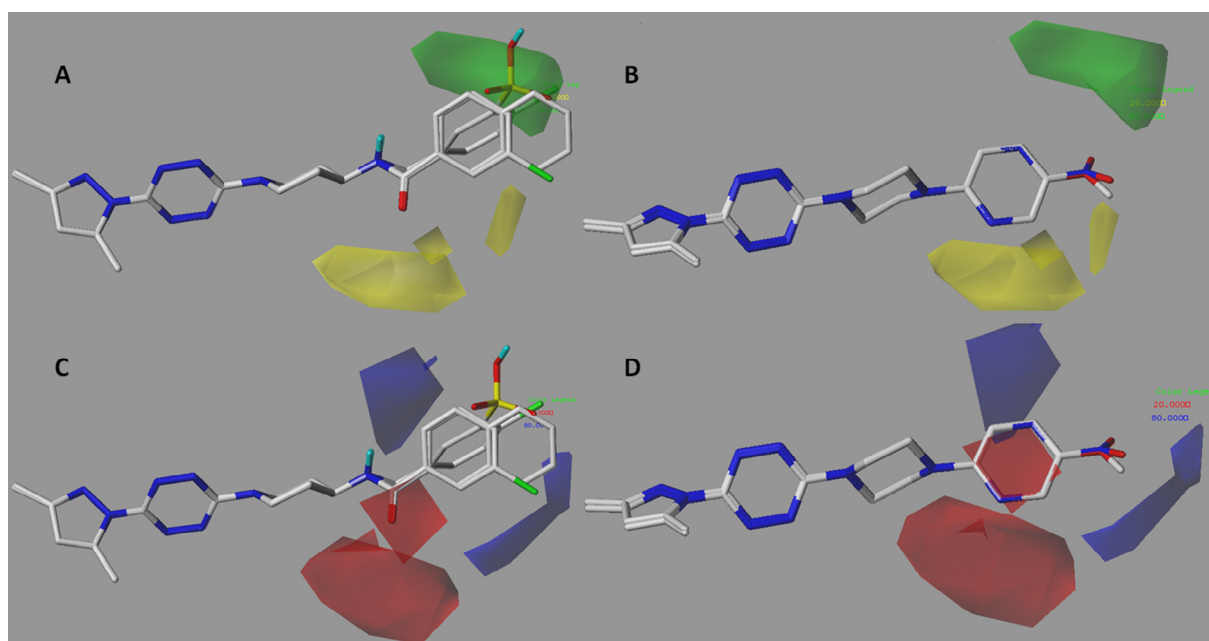


Fig. 4 3D-QSAR in HL60. CoMFA Steric (A, B) and electrostatic (C, D) contour maps around the most active compounds **1i**, **1j**, **1k** (left) and the less active compounds **2d**, **2i** and **2j** (right). The green contours mean that the presence of bulky groups favours biological activity, and in yellow, small substituents are also favourable. In red, electron-withdrawing substituents favour activity, and in blue electropositive substituents are favourable.

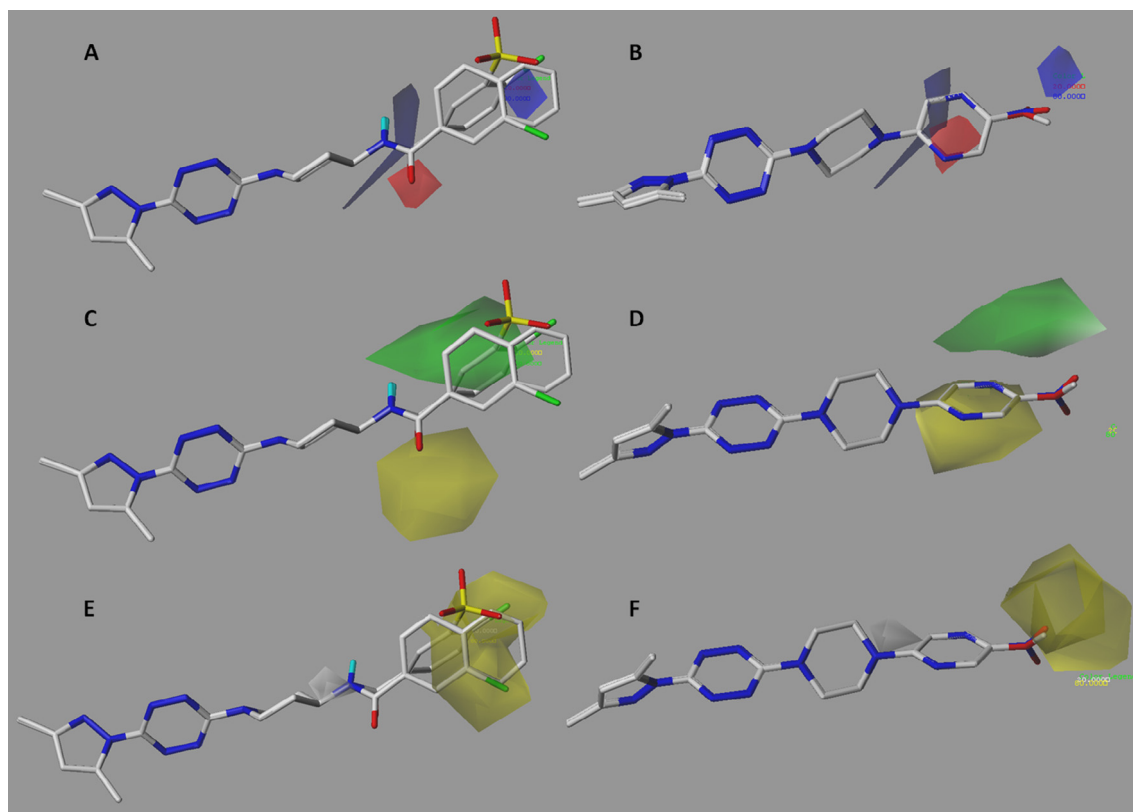


Fig. 5 CoMSIA in HL60. A and B are steric contour maps. C and D are electrostatic contour maps. E and F are hydrophobic contour maps of the most active compounds (**1i**, **1j** and **1k** (on the left)) and the least active (**2d**, **2i** and **2j** (on the right)). Green means that the presence of bulky groups favours biological activity, whereas yellow indicates that the use of small groups is also favourable. Red means that electronegative groups favour biological activity, and blue means that electropositive groups are also favourable. On hydrophobic maps (E and F), yellow means that using lipophilic substituents favours biological activity, while white polyhedrons mean that using hydrophilic substitutes is also favourable.

compounds. A white polyhedron is depicted around the nitrogen atom of the amide group. Thus, a reasonable modification would be the replacement of the amide by an amine protonable nitrogen.

On the other hand, the CoMFA and CoMSIA electrostatic contour maps show blue polyhedra around the peripheral phenyl moiety. That means the benzene ring should be substituted with electron withdrawing groups. Therefore, the use of a ketone instead of an amide linker would be beneficial. The replacement of the benzene ring for pyridine or their derivatives in **series I** should be explored. Only in the CoMFA electrostatic in HL60, two prominent red polyhedra are depicted near the carbonyl group in the amide of the most active compounds and surrounding the pyridine in the less active compounds. This suggests that a way to bolster the activity of these less active molecules is to replace the pyridine ring for activated phenyl rings.

2.6. Cell death mechanism assay

HCT116, HeLa, HL60 and H1975 cells lines were incubated for 16 h in the presence of 50 μM of the most promising tetrazine derivatives (compounds with the lowest

IC₅₀ values). By flow cytometry analysis, it was determined a population of viable cells impermeable to PI (propidium iodide; PI negative) and two populations of PI-permeable (PI positive) dead cells which were distinguished based on fluorescence intensity to either hypodiploid apoptotic cells or necrotic cells with intact DNA. As positive control, the same quantity of etoposide and vatalanib was used. The results are shown in Fig. 6. HCT116 cells shown both apoptosis and necrosis, being apoptosis the main cell death mechanism. A 40% of apoptosis was produced by **1c** and **1i**, with a similar behaviour than etoposide. In HL60 cells, cell death by necrosis is the main cell death mechanism. In Hela cells, it was observed a slow increase in apoptotic and necrotic cell death for all compounds studied in this cell line. H1975 cells shown both cell death mechanisms with an increase in necrosis in two compounds (**1j**, **1l**). In Vero cells, the main cell death is necrosis with the compound **1l**.

3. Conclusions

We synthesized and characterized two new series of 3,6-disubstituted-1,2,4,5-tetrazines which were studied in four cancer cell lines (H1975, HL-60, HCT116 and HeLa) and Vero cells. Our results

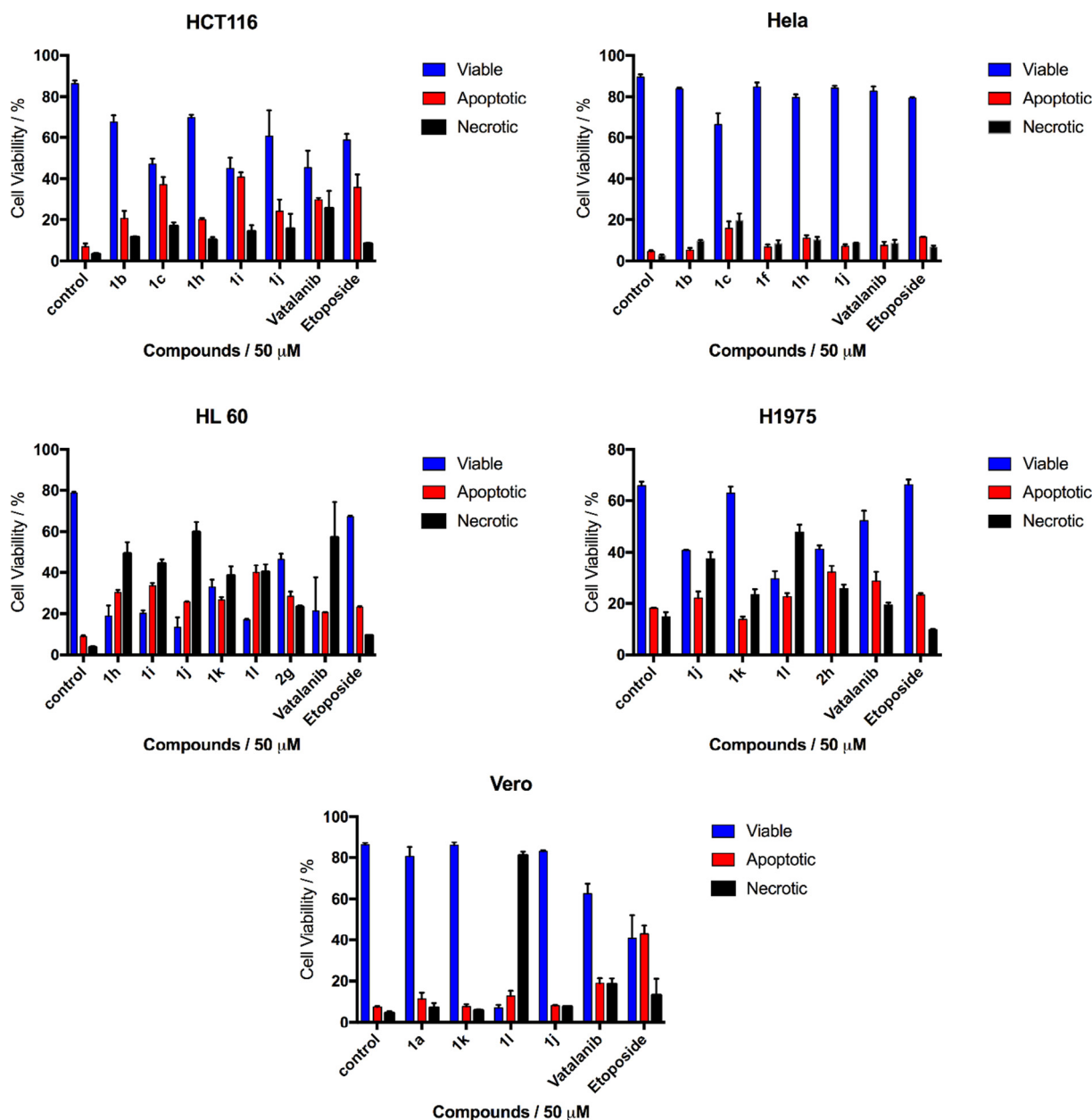


Fig. 6 Viability in different cancer cells lines treated with selected tetrazines. Cells were stimulated for 16 h with the different compounds (50 μ M). The cells were then stained with propidium iodide (PI; 10 μ g/ml) and cell viability and cell death by apoptosis or necrosis was evaluated by flow cytometry.

indicate that chemical changes in aromatic moiety can positively influence cytotoxicity and selectivity. Some of these compounds, especially **1f**, **1h**, **1i**, **1j**, **1k**, **1l** and **2h** were shown to be more potent than the drugs etoposide and vatalanib in some cancer cell lines, and more selective when compared with Vero cells. Preliminary evidence about some structure activity relationships was confirmed by *in silico* studies through the 3D-QSAR analysis. A 3D-QSAR equation for the activity on HL60 cells was obtained with a coefficient of determination $r^2 > 0.9$ and the contour maps for each cancer cell lines indicated that the cytotoxic activity was related to the steric and electronic features in the benzene ring. At the same time, the induction of apoptosis was the main mechanism of action observed for the most active compounds in HCT116 cell lines. Hence, **1f**, **1i**, **1j** and **2h** are interesting candidates for the development of new anticancer drugs.

4. Experimental

4.1. Materials and measurements

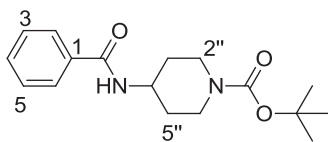
Melting points were determined on a Kofler Thermograte apparatus and were uncorrected. Infrared spectra were recorded on a JASCO FT/IR-400 spectrophotometer. Nuclear magnetic resonance (NMR) spectra were recorded, unless otherwise specified, on a Bruker AM-400 instrument using deuterated chloroform or dimethylsulphoxide solutions containing tetramethylsilane as an internal standard. Mass spectra were obtained on a HP 5988A mass spectrometer. HRMS-ESI-MS experiments were performed using a Thermo Scientific

Exacte Plus Orbitrap spectrometer with a constant nebulizer temperature of 250 °C. The experiments were carried out in positive or negative ion mode, with a scan range of m/z 300.00–1510.40 with a resolution of 140,000. The samples were infused directly into the ESI source, via a syringe pump, at flow rates of $5 \mu\text{L min}^{-1}$, through the instrument's injection valve. Thin layer chromatography (tlc) was performed using Merck GF-254 type 60 silica gel. Column chromatography was carried out using Merck type 9385 silica gel. The purity of the compounds was determined by tlc, NMR spectra and HRMS. For X-ray crystal structure analysis, data sets were collected with a STOE IPDS II two-circle-diffractometer using Mo K α radiation ($\lambda = 0.71073 \text{ \AA}$). The intensities were corrected for absorption by an empirical correction with X-Area. (Stoe&Cie, 2001). The structures were solved by direct methods (SHELXS) (Sheldrick, 2008) and refined by full-matrix least-squares calculations on F^2 (SHELXL-97). Anisotropic displacement parameters were refined for all non-hydrogen atoms. Selected crystallographic data are listed in Table S-1 (ESI).

4.2. Synthesis and characterization

4.2.1. General synthetic procedure of compounds 4a-l

tert-Butyl-4-aminopiperidine-1-carboxylate (*N*-Boc-4-aminopiperidine) (1 mmol) and the corresponding aryl chloride **3a-l** (1 mmol), were added to a reaction flask that contained dry THF and CH_2Cl_2 (1:1) and a small portion of molecular sieves. The mixture was stirred at room temperature overnight. Then the mixture was put in ice/water and diethyl ether (50 mL) was added. The organic extracts were washed with two portions of Na_2CO_3 ($2 \times 20 \text{ mL}$, 10%) and water ($2 \times 20 \text{ mL}$), and dried over Na_2SO_4 . The solution was evaporated to dryness and the crude product was purified by column chromatographic on silica gel using dichloromethane as eluent.



4.2.1.1. *tert*-Butyl-4-benzamidopiperidine-1-carboxylate (**4a**). Yield, 70%. White solid, mp 160–161 °C. $^1\text{H NMR}$ (400 MHz, CDCl_3) δ 7.56 (d, $J = 7.7 \text{ Hz}$, 2H, H2 + H6), 7.24 (m, 3H, H3, H4 + H5), 5.94 (d, $J = 7.4 \text{ Hz}$, 1H, NH), 3.98–3.90 (m, 3H, N-CH-pip + N- CH_2 -pip), 2.71 (t, $J = 12.2 \text{ Hz}$, 2H, N- CH_2 -pip), 1.82 (d, $J = 11.7 \text{ Hz}$, 2H, - CH_2 -pip), 1.27 (m, 11H, - CH_2 -pip + $3 \times \text{CH}_3$). $^{13}\text{C NMR}$ (101 MHz, CDCl_3) δ 166.91 (C=O), 154.75 (O=C=O), 134.55 (C1), 131.52 (C4), 128.58 (C3 + C5), 126.89 (C2 + C6), 79.73 (O-C), 47.25 (C4''), 42.79 (C2'' + C6''), 32.14 (C3'' + C5''), 28.44 ($3 \times \text{CH}_3$). IR (KBr, cm^{-1}): 3278, 2999, 1686, 1628, 1276, 696. HRMS for ($\text{C}_{17}\text{H}_{24}\text{N}_2\text{O}_3$ [M^-]). Calcd: 303.1714. Found: 303.1711.

4.2.1.2. *tert*-Butyl-4-[(3,5-dimethylbenzoyl)amino]piperidine-1-carboxylate (**4b**). Yield, 67%. White solid, mp 108–109 °C. $^1\text{H NMR}$ (400 MHz, CDCl_3) δ 7.23 (s, 2H, H2 + H6), 6.99 (s, 1H, H4), 6.04 (d, $J = 7.5 \text{ Hz}$, 1H, NH), 3.96

(d, $J = 11.6 \text{ Hz}$, 3H, N-CH-pip + N- CH_2 -pip), 2.77 (t, $J = 12.4 \text{ Hz}$, 2H, N- CH_2 -pip), 2.22 (s, 6H, $2 \times \text{CH}_3$), 1.87 (d, $J = 12.2 \text{ Hz}$, 2H, - CH_2 -pip), 1.38–1.23 (m, 11H, - CH_2 -pip + $3 \times \text{CH}_3$). $^{13}\text{C NMR}$ (101 MHz, CDCl_3) δ 167.24 (C=O), 154.72 (O=C=O), 138.23 (C3 + C5), 134.58 (C1), 133.03 (C4), 124.66 (C2 + C6), 79.64 (O-C), 47.12 (C4''), 42.77 (C2'' + C6''), 32.12 (C3'' + C5''), 28.43 ($3 \times \text{CH}_3$), 21.20 ($2 \times \text{CH}_3$). IR (KBr, cm^{-1}): 3253, 2930, 1689, 1633, 1313, 936, 726. HRMS for ($\text{C}_{19}\text{H}_{28}\text{N}_2\text{O}_3$ [M^-]). Calcd: 331.2027. Found: 331.2026.

4.2.1.3. *tert*-Butyl-4-[(3-chloro-5-fluorobenzoyl)amino]piperidine-1-carboxylate (**4c**). Yield, 77%. White solid, mp 129–131 °C. $^1\text{H NMR}$ (400 MHz, CDCl_3) δ 7.38 (s, 1H, H2), 7.24 (d, $J = 8.7 \text{ Hz}$, 1H, H4), 7.05 (d, $J = 8.0 \text{ Hz}$, 1H, H6), 6.21 (d, $J = 7.4 \text{ Hz}$, 1H, NH), 3.94 (d, $J = 5.4 \text{ Hz}$, 3H, N-CH-pip + N- CH_2 -pip), 2.72 (t, $J = 12.2 \text{ Hz}$, 2H, N- CH_2 -pip), 1.83 (d, $J = 11.9 \text{ Hz}$, 2H, - CH_2 -pip), 1.27 (m, 11H, - CH_2 -pip + $3 \times \text{CH}_3$). $^{13}\text{C NMR}$ (101 MHz, CDCl_3) δ 164.34 (d, $J_{CF} = 2.4 \text{ Hz}$, C=O), 162.54 (d, $J_{CF} = 251.6 \text{ Hz}$, C5), 154.70 (O=C=O), 137.76 (d, $J_{CF} = 7.5 \text{ Hz}$, C3), 135.49 (d, $J_{CF} = 10.0 \text{ Hz}$, C1), 123.12 (d, $J_{CF} = 3.2 \text{ Hz}$, C2), 119.07 (d, $J_{CF} = 24.8 \text{ Hz}$, C4), 112.98 (d, $J_{CF} = 22.9 \text{ Hz}$, C6), 79.84 (O-C), 47.64 (C4''), 42.77 (C2'' + C6''), 31.97 (C3'' + C5''), 28.42 ($3 \times \text{CH}_3$). $^{19}\text{F NMR}$ (376 MHz, CDCl_3) δ -109.55. IR (KBr, cm^{-1}): 3253, 3091, 1691, 1588, 1283, 1140, 738. HRMS for ($\text{C}_{17}\text{H}_{22}\text{ClFN}_2\text{O}_3$ [M^-]). Calcd: 355.1230. Found: 355.1226.

4.2.1.4. *tert*-Butyl-4-[[2-nitro-4-(trifluoromethyl)benzoyl]amino]piperidine-1-carboxylate (**4d**). Yield, 80%. White solid, mp 150–152 °C. $^1\text{H NMR}$ (400 MHz, CDCl_3) δ 8.43 (s, 1H, H3), 8.17 (d, $J = 4.7 \text{ Hz}$, 1H, H5), 7.97 (d, $J = 8.0 \text{ Hz}$, 1H, H6), 6.63 (s, 1H, NH), 4.32 (m, 1H, N-CH-pip), 3.54 (s, 2H, N- CH_2 -pip), 2.47 (t, $J = 8.1 \text{ Hz}$, 2H, N- CH_2 -pip), 2.23 (dd, $J = 15.3, 7.6 \text{ Hz}$, 2H, - CH_2 -pip), 1.75–1.67 (m, 2H, - CH_2 -pip), 1.55 (s, 9H, $3 \times \text{CH}_3$). $^{13}\text{C NMR}$ (101 MHz, CDCl_3) δ 165.63 (C=O), 154.74 (O=C=O), 146.15 (C2), 135.33 (C1), 133.58 (d, $J_{CF} = 34.5 \text{ Hz}$, C4), 130.72 (C6), 129.75 (q, $J_{CF} = 3.3 \text{ Hz}$, C3), 126.41 (CF₃), 121.10 (d, $J_{CF} = 3.8 \text{ Hz}$, C5), 77.22 (O-C), 47.37 (C4''), 44.62 (C2'' + C6''), 43.61 (C3'' + C5''), 27.68 ($3 \times \text{CH}_3$). $^{19}\text{F NMR}$ (376 MHz, CDCl_3) δ -63.10. IR (KBr, cm^{-1}): 3293, 1695, 1643, 1551, 1421, 1180. HRMS for ($\text{C}_{18}\text{H}_{22}\text{F}_3\text{N}_3\text{O}_5$ [M^-]). Calcd: 416.1433. Found: 416.1440.

4.2.1.5. *tert*-Butyl-4-[(3-fluoro-4-methoxybenzoyl)amino]piperidine-1-carboxylate (**4e**). Yield, 74%. White solid, mp 177–179 °C. $^1\text{H NMR}$ (400 MHz, CDCl_3) δ 7.49 (br.s, 2H, H2 + H6), 6.90 (t, $J = 8.2 \text{ Hz}$, 1H, H5), 6.19 (d, $J = 7.5 \text{ Hz}$, 1H, NH), 4.04 (d, $J = 11.6 \text{ Hz}$, 3H, N-CH-pip + N- CH_2 -pip), 3.87 (s, 3H, OCH₃), 2.83 (t, $J = 12.6 \text{ Hz}$, 2H, N- CH_2 -pip), 1.94 (d, $J = 12.2 \text{ Hz}$, 2H, - CH_2 -pip), 1.46–1.29 (m, 11H, - CH_2 -pip + $3 \times \text{CH}_3$). $^{13}\text{C NMR}$ (101 MHz, CDCl_3) δ 165.31 (C=O), 154.71 (O=C=O), 151.86 (d, $J_{CF} = 247.4 \text{ Hz}$, C3), 150.38 (d, $J_{CF} = 10.7 \text{ Hz}$, C4), 127.29 (d, $J_{CF} = 5.4 \text{ Hz}$, C1), 123.49 (d, $J_{CF} = 3.5 \text{ Hz}$, C6), 115.06 (d, $J_{CF} = 19.7 \text{ Hz}$, C2), 112.62 (d, $J_{CF} = 1.8 \text{ Hz}$, C5), 79.71 (O-C), 56.26 (OCH₃), 47.34 (C4''), 42.79 (C2'' + C6''), 32.10 (C3'' + C5''), 28.42 ($3 \times \text{CH}_3$). $^{19}\text{F NMR}$ (376 MHz, DMSO- d_6) δ -134.96. IR (KBr, cm^{-1}): 3384, 2947, 1692, 1632, 1281,

1019, 764. HRMS for (C₁₈H₂₅FN₂O₄ [M⁻]). Calcd: 351.1726. Found: 351.1723.

4.2.1.6. *tert*-Butyl-4-[(4-cyanobenzoyl)amino]piperidine-1-carboxylate (**4f**). Yield, 71%. White solid, mp 182–183 °C. ¹H NMR (400 MHz, CDCl₃) δ 7.99 (d, *J* = 7.9 Hz, 2H, C3'' + C5''), 7.71 (d, *J* = 7.8 Hz, 2H, C2'' + C6''), 6.40 (d, *J* = 7.0 Hz, 1H, NH), 4.10 (m, 3H, N-CH-pip + N-CH₂-pip), 2.87 (s, 2H, N-CH₂-pip), 1.94 (d, *J* = 12.0 Hz, 2H, -CH₂-pip), 1.45 (s, 11H, -CH₂-pip + 3 × CH₃). ¹³C NMR (101 MHz, CDCl₃) δ 165.07 (C=O), 154.60 (O=C=O), 138.68 (C1), 131.86 (C3 + C5), 128.17 (C2 + C6), 118.09 (CN), 115.01 (C4), 79.35 (O-C), 47.41 (C4''), 42.73 (C2'' + C6''), 31.41 (C3'' + C5''), 28.27 (3 × CH₃). IR (KBr, cm⁻¹): 3359, 2982, 2230, 1693, 1641, 1430, 1302, 864, 769. HRMS for (C₁₈H₂₃N₃O₃ [M + H]⁺). Calcd: 328.1667. Found: 328.1663.

4.2.1.7. *tert*-Butyl-4-[(2-methylbenzoyl)amino]piperidine-1-carboxylate (**4g**). Yield, 83%. White solid, mp 103–104 °C. ¹H NMR (400 MHz, CDCl₃) δ 7.33 (d, *J* = 6.8 Hz, 2H, H4 + H6), 7.22 (d, *J* = 7.5 Hz, 2H, H3 + H5), 7.08 (s, 1H, NH), 4.10 (m, 3H, N-CH-pip + N-CH₂-pip), 2.92 (s, 2H, N-CH₂-pip), 2.44 (s, 3H, CH₃), 1.99 (d, *J* = 12.3 Hz, 2H, -CH₂-pip), 1.48 (s, 11H, -CH₂-pip + 3 × CH₃). ¹³C NMR (101 MHz, CDCl₃) δ 169.52 (C=O), 154.56 (O=C=O), 136.96 (C1), 135.49 (C2), 130.56 (C4), 129.39 (C3), 126.80 (C6), 125.46 (C5), 79.35 (O-C), 46.80 (C4''), 42.31 (C2'' + C6''), 31.65 (C3'' + C5''), 28.30 (3 × CH₃), 19.48 (CH₃). IR (KBr, cm⁻¹): 3271, 2929, 1692, 1634, 1429, 1145, 740. HRMS for (C₁₈H₂₆N₂O₃ [M⁻]). Calcd: 317.1871. Found: 317.1870.

4.2.1.8. *tert*-Butyl-4-[(2-bromobenzoyl)amino]piperidine-1-carboxylate (**4h**). Yield, 75%. White solid, mp 64–65 °C. ¹H NMR (400 MHz, CDCl₃) δ 7.53 (d, *J* = 7.9 Hz, 1H, H6), 7.47 (d, *J* = 7.0 Hz, 1H, H3), 7.31 (t, *J* = 7.0 Hz, 1H, H4), 7.23 (t, *J* = 7.5 Hz, 1H, H5), 5.95 (s, 1H, NH), 4.06 (m, 3H, N-CH-pip + N-CH₂-pip), 2.90 (t, *J* = 11.5 Hz, 2H, N-CH₂-pip), 2.00 (d, *J* = 11.6 Hz, 2H, -CH₂-pip), 1.42 (s, 11H, -CH₂-pip + 3 × CH₃). ¹³C NMR (101 MHz, CDCl₃) δ 166.94 (C=O), 154.69 (O=C=O), 137.74 (C1), 133.33 (C3), 131.29 (C5), 129.59 (C4), 127.62 (C6), 119.20 (C2), 79.72 (O-C), 47.42 (C4''), 42.31 (C2'' + C6''), 31.81 (C3'' + C5''), 28.43 (3 × CH₃). IR (KBr, cm⁻¹): 3242, 3066, 1689, 1591, 1431, 743. HRMS for (C₁₇H₂₃BrN₂O₃ [M + H]⁺). Calcd: 381.0819. Found: 381.0825.

4.2.1.9. *tert*-Butyl-4-(2-naphthoylamino)piperidine-1-carboxylate (**4i**). Yield, 82%. White solid, mp 156–158 °C. ¹H NMR (400 MHz, CDCl₃) δ 8.22 (s, 1H, H2), 7.92–7.78 (m, 4H, H3, H6, H7, H8), 7.62–7.41 (m, 2H, H4 + H5), 6.27 (s, 1H, NH), 4.22–4.08 (m, 3H, N-CH-pip + N-CH₂-pip), 2.87 (t, *J* = 12.1 Hz, 2H, N-CH₂-pip), 2.01 (d, *J* = 11.0 Hz, 2H, -CH₂-pip), 1.55–1.35 (m, 11H, -CH₂-pip + 3 × CH₃). ¹³C NMR (101 MHz, CDCl₃) δ 166.94 (C=O), 154.75 (O=C=O), 134.73 (C1), 132.60 (C2a), 131.79 (C6a), 128.88 (C3), 128.46 (C5), 127.75 (C2), 127.67 (C7), 127.33 (C6), 126.79 (C4), 123.57 (C8), 79.72 (O-C), 47.37 (C4''), 42.78 (C2'' + C6''), 32.18 (C3'' + C5''), 28.45 (3 × CH₃). IR (KBr, cm⁻¹): 3267, 2951, 1701, 1685, 1307, 778. HRMS for (C₂₁H₂₆N₂O₃ [M⁻]). Calcd: 353.1865. Found: 353.1871.

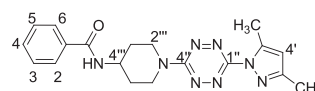
4.2.1.10. *tert*-Butyl-4-[(3-chlorobenzoyl)amino]piperidine-1-carboxylate (**4j**). Yield, 65%. White solid, mp 135–137 °C. ¹H NMR (400 MHz, CDCl₃) δ 7.62 (s, 1H, H2), 7.51 (d, *J* = 7.7 Hz, 1H, H4), 7.34 (d, *J* = 8.1 Hz, 1H, H6), 7.23 (t, *J* = 7.8 Hz, 1H, H5), 6.12 (d, *J* = 7.6 Hz, 1H, NH), 4.09–3.87 (m, 3H, N-CH-pip + N-CH₂-pip), 2.76 (t, *J* = 12.4 Hz, 2H, N-CH₂-pip), 1.96–1.82 (m, 2H, -CH₂-pip), 1.41–1.21 (m, 11H, -CH₂-pip + 3 × CH₃). ¹³C NMR (101 MHz, CDCl₃) δ 165.54 (C=O), 154.71 (O=C=O), 136.35 (C1), 134.70 (C3), 131.50 (C4), 129.88 (C5), 127.28 (C6), 125.08 (C2), 79.76 (O-C), 47.46 (C4''), 42.78 (C2'' + C6''), 32.04 (C3'' + C5''), 28.43 (3 × CH₃). IR (KBr, cm⁻¹): 3273, 2979, 1795, 1692, 1428, 1304, 750. HRMS for (C₁₇H₂₃ClN₂O₃ [M⁻]). Calcd: 337.1324. Found: 337.1326.

4.2.1.11. *tert*-Butyl-4-(4-chloro-3-sulfamoylbenzamido)piperidine-1-carboxylate (**4k**). Yield, 77%. Brown oil. ¹H NMR (400 MHz, DMSO-*d*₆) δ 7.75 (d, *J* = 3.6 Hz, 1H, H6), 7.53 (d, *J* = 4.9 Hz, 1H, H4), 7.07 (t, *J* = 4.3 Hz, 1H, NH), 6.13 (s, 1H, H3), 4.84 (br.s, 2H, NH₂), 4.36–4.17 (m, 1H, N-CH-pip), 3.37 (t, *J* = 11.8 Hz, 2H, N-CH₂-pip), 2.13 (d, *J* = 10.2 Hz, 2H, N-CH₂-pip), 1.74 (d, *J* = 8.5 Hz, 2H, -CH₂-pip), 1.25 (br.s, 11H, -CH₂-pip + 3 × CH₃). ¹³C NMR (101 MHz, CDCl₃) δ 163.64 (C=O), 161.55 (O=C=O), 134.78 (C3), 132.01 (C4), 130.00 (C1), 128.45 (C2), 127.60 (C5), 127.42 (C6), 79.19 (O-C), 47.02 (C4''), 44.36 (C2'' + C6''), 31.53 (C3'' + C5''), 28.22 (3 × CH₃). IR (KBr, cm⁻¹): 3349, 2952, 1672, 1637, 1531, 1431, 736. HRMS for (C₁₇H₂₄ClN₃O₅S [M⁻]). Calcd: 416.1052. Found: 416.1112.

4.2.1.12. *tert*-Butyl-4-{[4-(chloromethyl)benzoyl]amino}piperidine-1-carboxylate (**4l**). Yield, 65%, white solid; mp: 159–162 °C. ¹H NMR (400 MHz, CDCl₃) δ 7.96 (d, *J* = 7.9 Hz, 2H, H2 + H6), 7.38 (d, *J* = 7.9 Hz, 2H, H3 + H5), 4.55 (br, 2H, CH₂), 4.02 (m, 3H, N-CH-pip + N-CH₂-pip), 2.81 (t, *J* = 12.8 Hz, 2H, N-CH₂-pip), 1.97 (d, *J* = 11.1 Hz, 2H, -CH₂-pip), 1.42 (s, 11H, -CH₂-pip + 3 × CH₃). ¹³C NMR (50 MHz, DMSO-*d*₆) δ 162.65 (C=O), 161.15 (O=C=O), 136.59 (C4), 129.49 (C1), 125.61 (C3 + C5), 123.06 (C2 + C6), 74.20 (O-C), 41.98 (C-Cl), 40.14 (C4''), 37.47 (C2'' + C6''), 26.51 (C3'' + C5''), 23.09 (3 × CH₃). IR (KBr, cm⁻¹): 3312, 2971, 1690, 1636, 1425, 711. HRMS for (C₁₈H₂₅ClN₂O₃ [M⁻]). Calcd: 351.1481. Found: 351.1482.

4.2.2. General synthetic procedure of compounds **1a-l**

The protective Boc groups were removed from the **4a-l** compounds using TFA (Trifluoroacetic acid) (15 mmol) and TES (Triethylsilane) (3 mmol) as solvent at room temperature for 30 min. Once TFA and TES are removed, the free amine **5a-l** obtained was used without further purification. Finally, this amine (1 mmol) was mixed with tetrazine **6** (1 mmol) in acetonitrile (40 mL), an excess of TEA (3 mmol) and was stirred overnight at room temperature. After completion of the reaction, the mixture was concentrated. The solid residue was purified by column chromatography on silica gel using CH₂Cl₂/Acetone (5:1) as eluent to yield **1a-l**.



4.2.2.1. *N*-(1-(6-(3,5-dimethyl-1H-pyrazol-1-yl)-1,2,4,5-tetrazin-3-yl)piperidin-4-yl)benzamide (**1a**). Yield, 30%. Red solid, mp 172–174 °C. ¹H NMR (400 MHz, CDCl₃) δ 7.60 (d, *J* = 5.0 Hz, 2H, H₂ + H₆), 7.31–7.23 (m, 3H, H₃, H₄ + H₅), 6.25 (d, *J* = 6.2 Hz, 1H, NH), 5.91 (s, 1H, H₄'), 4.71 (d, *J* = 11.2 Hz, 2H, N-CH₂-pip), 4.19 (s, 1H, N-CH-pip), 3.13 (d, *J* = 9.9 Hz, 2H, N-CH₂-pip), 2.38 (d, *J* = 2.2 Hz, 3H, CH₃), 2.14 (d, *J* = 2.5 Hz, 3H, CH₃), 2.06 (d, *J* = 9.2 Hz, 2H, -CH₂-pip) 1.44 (d, *J* = 11.0 Hz, 2H, -CH₂-pip). ¹³C NMR (101 MHz, CDCl₃) δ 167.04 (C=O), 160.25 (C^{4'}), 156.68 (C^{1''}), 152.04 (C^{5'}), 141.89 (C^{3'}), 134.35 (C¹), 131.59 (C⁴), 128.56 (C³ + C⁵), 126.96 (C² + C⁶), 109.61 (C^{4'}), 47.11 (C^{4'''}), 42.94 (C^{2'''} + C^{6'''}), 31.64 (C^{3'''} + C^{5'''}), 13.68 (CH₃), 13.44 (CH₃). IR (KBr, cm⁻¹): 3274, 1629, 1556, 1534. HRMS for (C₁₉H₂₃N₈O [M + H]⁺). Calcd: 379.1995. Found: 379.1989.

4.2.2.2. *N*-(1-(6-(3,5-dimethyl-1H-pyrazol-1-yl)-1,2,4,5-tetrazin-3-yl)piperidin-4-yl)-3,5-dimethylbenzamide (**1b**). Yield, 34%. Red solid, mp 205–207 °C. ¹H NMR (400 MHz, CDCl₃) δ 7.23 (s, 2H, H₂ + H₆), 6.97 (s, 1H, H₄), 6.22 (d, *J* = 7.6 Hz, 1H, NH), 5.95 (s, 1H, H₄'), 4.75 (d, *J* = 13.7 Hz, 2H, N-CH₂-pip), 4.30–4.14 (m, 1H, N-CH-pip), 3.27–3.12 (m, 2H, N-CH₂-pip), 2.42 (s, 3H, CH₃), 2.19 (s, 9H, 3 × CH₃), 2.13–2.07 (m, 2H, -CH₂-pip), 1.53–1.43 (m, 2H, -CH₂-pip). ¹³C NMR (101 MHz, CDCl₃) δ 167.45 (C=O), 160.25 (C^{4''}), 156.66 (C^{1''}), 152.01 (C^{5'}), 141.88 (C^{3'}), 138.26 (C³ + C⁵), 134.31 (C¹), 133.16 (C⁴), 124.72 (C² + C⁶), 109.58 (C^{4'}), 47.00 (C^{4'''}), 42.94 (C^{2'''} + C^{6'''}), 31.66 (C^{3'''} + C^{5'''}), 21.18 (2 × CH₃), 13.66 (CH₃), 13.41 (CH₃). IR (KBr, cm⁻¹): 3287, 1634, 1536, 1483. HRMS for (C₂₁H₂₆N₈O [M + H]⁺). Calcd: 407.2308. Found: 407.2302.

4.2.2.3. 3-Chloro-*N*-(1-(6-(3,5-dimethyl-1H-pyrazol-1-yl)-1,2,4,5-tetrazin-3-yl)piperidin-4-yl)-5-fluorobenzamide (**1c**). Yield, 34%. Red solid, mp 194–196 °C. ¹H NMR (400 MHz, CDCl₃) δ 7.64 (s, 1H, H₄), 7.49 (d, *J* = 8.8 Hz, 1H, H₂), 7.22 (d, *J* = 8.0 Hz, 1H, H₆), 7.12 (d, *J* = 7.7 Hz, 1H, NH), 6.12 (s, 1H, H₄'), 4.95 (d, *J* = 13.7 Hz, 2H, N-CH₂-pip), 4.50–4.40 (m, 1H, N-CH-pip), 3.37 (t, *J* = 12.2 Hz, 2H, N-CH₂-pip), 2.61 (s, 3H, CH₃), 2.32–2.20 (m, 5H, CH₃ + -CH₂-pip), 1.78–1.67 (m, 2H, -CH₂-pip). ¹³C NMR (101 MHz, CDCl₃) δ 164.63 (d, *J*_{CF} = 2.5 Hz, C=O), 162.42 (d, *J*_{CF} = 251.3 Hz, C⁵), 160.19 (C^{4''}), 156.62 (C^{1''}), 152.03 (C^{5'}), 142.02 (C^{3'}), 137.69 (d, *J*_{CF} = 7.4 Hz, C³), 135.28 (d, *J*_{CF} = 10.1 Hz, C¹), 123.36 (d, *J*_{CF} = 3.1 Hz, C⁴), 118.95 (d, *J*_{CF} = 24.9 Hz, C⁶), 113.10 (d, *J*_{CF} = 23.0 Hz, C²), 109.70 (C^{4'}), 47.44 (C^{4'''}), 42.97 (C^{2'''} + C^{6'''}), 31.35 (C^{3'''} + C^{5'''}), 13.52 (CH₃), 13.44 (CH₃). ¹⁹F NMR (188 MHz, CDCl₃) δ -109.22. IR (KBr, cm⁻¹): 3261, 1638, 1537, 1484. HRMS for (C₁₉H₂₀ClFN₈O [M + H]⁺). Calcd: 431.1511. Found: 431.1505.

4.2.2.4. *N*-(1-(6-(3,5-dimethyl-1H-pyrazol-1-yl)-1,2,4,5-tetrazin-3-yl)piperidin-4-yl)-2-nitro-4-(trifluoromethyl)benzamide (**1d**). Yield, 55%. Red solid, mp 230–231 °C. ¹H NMR (400 MHz, CDCl₃) δ 8.26 (s, 1H, H₃), 7.85 (d, *J* = 7.8 Hz, 1H, H₅), 7.63 (d, *J* = 7.9 Hz, 1H, H₆), 6.54 (d, *J* = 6.5 Hz, 1H, NH), 6.00 (s, 1H, H₄'), 4.84 (d, *J* = 13.7 Hz, 2H, N-CH₂-pip), 4.44–4.31 (m, 1H, N-CH-pip), 3.36 (t, *J* = 12.1 Hz, 2H, N-CH₂-pip), 2.49 (s, 3H, CH₃), 2.33–2.18 (m, 5H, CH₃ + -CH₂-pip), 1.73–1.51 (m, 2H, -CH₂-pip). ¹³C

NMR (101 MHz, CDCl₃) δ 164.77 (C=O), 160.32 (C^{4''}), 156.65 (C^{1''}), 152.03 (C^{5'}), 146.34 (C²), 141.96 (C^{3'}), 135.88 (C¹), 131.45 (C⁵), 131.42 (C³), 130.39 (C⁶), 129.84 (CF₃), 121.93 (q, *J*_{CF} = 7.8 Hz, C⁴), 109.63 (C^{4'}), 47.55 (C^{4'''}), 42.81 (C^{2'''} + C^{6'''}), 31.09 (C^{3'''} + C^{5'''}), 13.63 (CH₃), 13.41 (CH₃). ¹⁹F NMR (188 MHz, CDCl₃) δ -63.11. IR (KBr, cm⁻¹): 3267, 1646, 1543, 1326. HRMS for (C₂₀H₂₀F₃N₉O₃ [M + H]⁺). Calcd: 492.1719. Found: 492.1717.

4.2.2.5. *N*-(1-(6-(3,5-dimethyl-1H-pyrazol-1-yl)-1,2,4,5-tetrazin-3-yl)piperidin-4-yl)-3-fluoro-4-methoxybenzamide (**1e**). Yield, 46%. Red Solid, mp 229–230 °C. ¹H NMR (400 MHz, CDCl₃) δ 7.50 (d, *J* = 10.1 Hz, 2H, H₂ + H₆), 6.88 (t, *J* = 8.0 Hz, 1H, H₅), 6.45 (d, *J* = 7.0 Hz, 1H, NH), 6.03 (s, 1H, H₄'), 4.84 (d, *J* = 13.2 Hz, 2H, N-CH₂-pip), 4.32 (br, 1H, N-CH-pip), 3.86 (s, 3H, OCH₃), 3.26 (t, *J* = 12.3 Hz, 2H, N-CH₂-pip), 2.50 (s, 1H, CH₃), 2.31–2.03 (m, 5H, CH₃ + -CH₂-pip), 1.56 (d, *J* = 10.2 Hz, 2H, -CH₂-pip). ¹³C NMR (101 MHz, CDCl₃) δ 165.49 (C=O), 160.19 (C^{4''}), 156.63 (C^{1''}), 152.01 (C^{5'}), 151.74 (d, *J*_{CF} = 247.0 Hz, C³), 150.41 (d, *J*_{CF} = 10.7 Hz, C⁴), 141.91 (C^{3'}), 127.07 (d, *J*_{CF} = 5.5 Hz, C¹), 123.54 (d, *J*_{CF} = 3.3 Hz, C⁶), 115.14 (d, *J*_{CF} = 19.7 Hz, C²), 112.56 (d, *J*_{CF} = 1.5 Hz, C⁵), 109.59 (C^{4'}), 56.23 (OCH₃), 47.17 (C^{4'''}), 42.95 (C^{2'''} + C^{6'''}), 31.57 (C^{3'''} + C^{5'''}), 13.62 (CH₃), 13.38 (CH₃). ¹⁹F NMR (188 MHz, CDCl₃) δ -133.85. IR (KBr, cm⁻¹): 3261, 1631, 1541, 1485. HRMS for (C₂₀H₂₃FN₈O₂ [M + H]⁺). Calcd: 427.2006. Found: 427.2003.

4.2.2.6. 4-Cyano-*N*-(1-(6-(3,5-dimethyl-1H-pyrazol-1-yl)-1,2,4,5-tetrazin-3-yl)piperidin-4-yl)benzamide (**1f**). Yield, 30%. Red solid, mp 187–189 °C. ¹H NMR (400 MHz, CDCl₃) δ 7.88 (d, *J* = 8.1 Hz, 2H, H₂ + H₆), 7.65 (d, *J* = 8.0 Hz, 2H, H₃ + H₅), 6.78 (d, *J* = 7.6 Hz, 1H, NH), 6.04 (s, 1H, H₄'), 4.86 (d, *J* = 13.7 Hz, 2H, N-CH₂-pip), 4.44–4.30 (m, 1H, N-CH-pip), 3.28 (t, *J* = 12.2 Hz, 2H, N-CH₂-pip), 2.52 (s, 3H, CH₃), 2.21–2.19 (m, 5H, CH₃ + -CH₂-pip), 1.65–1.54 (m, 2H, -CH₂-pip). ¹³C NMR (101 MHz, CDCl₃) δ 165.26 (C=O), 160.22 (C^{4''}), 156.68 (C^{1''}), 152.09 (C^{5'}), 142.01 (C^{3'}), 138.32 (C¹), 132.31 (C³ + C⁵), 127.89 (C² + C⁶), 118.02 (CN), 115.03 (C⁴), 109.75, 47.49 (C^{4'''}), 43.01 (C^{2'''} + C^{6'''}), 31.43 (C^{3'''} + C^{5'''}), 13.56 (CH₃), 13.48 (CH₃). IR (KBr, cm⁻¹): 3261, 1636, 1534, 1485. HRMS for (C₂₀H₂₂N₉O [M + H]⁺). Calcd: 404.1947. Found: 404.1940.

4.2.2.7. *N*-(1-(6-(3,5-dimethyl-1H-pyrazol-1-yl)-1,2,4,5-tetrazin-3-yl)piperidin-4-yl)-2-methylbenzamide (**1g**). Yield, 36%. Red solid, mp 204–206 °C. ¹H NMR (400 MHz, CDCl₃) δ 7.37–7.30 (m, 2H, H₄ + H₆), 7.25–7.19 (m, 2H, H₃ + H₅), 6.12 (s, 1H, H₄'), 6.00 (d, *J* = 7.7 Hz, 1H, NH), 4.92 (d, *J* = 13.8 Hz, 2H, N-CH₂-pip), 4.46–4.30 (m, 1H, N-CH-pip), 3.45–3.32 (m, 2H, N-CH₂-pip), 2.59 (s, 3H, CH₃), 2.47 (s, 3H, CH₃), 2.37 (s, 3H, CH₃), 2.33–2.24 (m, 2H, -CH₂-pip), 1.67–1.57 (m, 2H, -CH₂-pip). ¹³C NMR (101 MHz, CDCl₃) δ 169.61 (C=O), 160.28 (C^{4''}), 156.71 (C^{1''}), 152.05 (C^{5'}), 141.88 (C^{3'}), 136.19 (C¹), 135.89 (C²), 131.01 (C⁴), 129.97 (C³), 126.60 (C⁶), 125.74 (C⁵), 109.62 (C^{4'}), 46.88 (C^{4'''}), 42.86 (C^{2'''} + C^{6'''}), 31.63 (C^{3'''} + C^{5'''}), 19.71 (CH₃), 13.70 (CH₃), 13.45 (CH₃). IR (KBr, cm⁻¹): 3277, 1629, 1550, 1485. HRMS for (C₂₀H₂₄N₈O [M + H]⁺). Calcd: 393.2151. Found: 393.2146.

4.2.2.8. *2-Bromo-N-(1-(6-(3,5-dimethyl-1H-pyrazol-1-yl)-1,2,4,5-tetrazin-3-yl)piperidin-4-yl)benzamide (Ih)*. Yield, 35%. Red solid, mp 134–136 °C. ¹H NMR (400 MHz, CDCl₃) δ 7.45 (d, *J* = 7.9 Hz, 1H, H6), 7.39 (dd, *J* = 7.6, 1.5 Hz, 1H, H3), 7.23 (t, *J* = 7.4 Hz, 1H, H4), 7.15 (td, *J* = 7.7, 1.6 Hz, 1H, H5), 6.20 (d, *J* = 7.8 Hz, 1H, NH), 5.98 (s, 1H, H4'), 4.74 (d, *J* = 13.8 Hz, 2H, N-CH₂-pip), 4.34–4.21 (m, 1H, N-CH-pip), 3.36–3.24 (m, 2H, N-CH₂-pip), 2.45 (s, 3H, CH₃), 2.23 (s, 3H, CH₃), 2.16 (dd, *J* = 13.0, 2.8 Hz, 2H, -CH₂-pip), 1.63–1.48 (m, 2H, -CH₂-pip). ¹³C NMR (101 MHz, CDCl₃) δ 167.11 (C=O), 160.28 (C4''), 156.67 (C1''), 152.02 (C5'), 141.86 (C3'), 137.60 (C1), 133.27 (C3), 131.30 (C5), 129.48 (C4), 127.56 (C6), 119.20 (C2), 109.61 (C4'), 47.19 (C4''), 42.72 (C2''' + C6'''), 31.32 (C3''' + C5'''), 13.71 (CH₃), 13.45 (CH₃). IR (KBr, cm⁻¹): 3253, 1646, 1544. HRMS for (C₁₉H₂₁BrN₈O [M + H]⁺). Calcd: 457.1100. Found: 457.1097.

4.2.2.9. *N-(1-[6-(3,5-dimethyl-1H-pyrazol-1-yl)-1,2,4,5-tetrazin-3-yl]piperidin-4-yl)-2-naphthamide (Ii)*. Yield, 66%. Red solid, mp 204–206 °C. ¹H NMR (400 MHz, CDCl₃) δ 8.25 (s, 1H, H2), 7.82–7.78 (m, 4H, H3, H6, H7, H8), 7.51–7.46 (m, 2H, H4 + H5), 6.49 (br, 1H, NH), 6.04 (s, 1H, H4'), 4.85 (d, *J* = 12.1 Hz, 2H, N-CH₂-pip), 4.39 (br, 1H, N-CH-pip), 3.27 (t, *J* = 12.4 Hz, 2H, N-CH₂-pip), 2.51 (s, 3H, CH₃), 2.28 (s, 3H, CH₃), 2.23 (d, *J* = 11.3 Hz, 2H, -CH₂-pip), 1.61 (d, *J* = 9.6 Hz, 2H, -CH₂-pip). ¹³C NMR (101 MHz, CDCl₃) δ 167.12 (C=O), 160.26 (C4''), 156.70 (C1''), 152.06 (C5'), 141.91 (C3'), 134.76 (C1), 132.56 (C2a), 131.57 (C6a), 128.87 (C3), 128.46 (C5), 127.75 (C2 + C7), 127.47 (C6), 126.81 (C4), 123.58 (C8), 109.63 (C4'), 47.22 (C4''), 42.96 (C2''' + C6'''), 29.70 (C3''' + C5'''), 13.70 (CH₃), 13.45 (CH₃). IR (KBr, cm⁻¹): 3265, 1637, 1543, 1490, 1236. HRMS (for C₂₃H₂₅N₈O [M + H]⁺). Calcd: 429.2151. Found: 429.2141.

4.2.2.10. *3-Chloro-N-(1-(6-(3,5-dimethyl-1H-pyrazol-1-yl)-1,2,4,5-tetrazin-3-yl)piperidin-4-yl)benzamide (Ij)*. Yield, 69%. Red solid, mp 179–181 °C. ¹H NMR (400 MHz, CDCl₃) δ 7.70 (s, 1H, H2), 7.58 (d, *J* = 7.8 Hz, 1H, H4), 7.35 (d, *J* = 8.1 Hz, 1H, H6), 7.23 (t, *J* = 8.0 Hz, 1H, H5), 6.76 (d, *J* = 7.6 Hz, 1H, NH), 5.99 (s, 1H, H4'), 4.80 (d, *J* = 13.8 Hz, 2H, N-CH₂-pip), 4.36–4.26 (m, 1H, N-CH-pip), 3.30–3.17 (m, 2H, N-CH₂-pip), 2.47 (s, 3H, CH₃), 2.19 (s, 3H, CH₃), 2.14 (dd, *J* = 13.0, 2.8 Hz, 2H, -CH₂-pip), 1.56 (qd, *J* = 12.3, 4.1 Hz, 2H, -CH₂-pip). ¹³C NMR (101 MHz, CDCl₃) δ 165.80 (C=O), 160.20 (C4''), 156.62 (C1''), 152.01 (C5'), 141.94 (C3'), 136.20 (C1), 134.54 (C3), 131.45 (C4), 129.78 (C5), 127.43 (C6), 125.23 (C2), 109.65 (C4'), 47.29 (C4''), 42.94 (C2''' + C6'''), 31.45 (C3''' + C5'''), 13.59 (CH₃), 13.44 (CH₃). IR (KBr, cm⁻¹): 3255, 1639, 1540, 1484. HRMS for (C₁₉H₂₂ClN₈O [M + H]⁺). Calcd: 413.1605. Found: 413.1488.

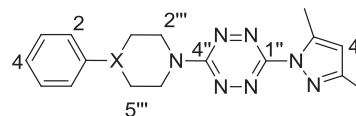
4.2.2.11. *4-Chloro-N-(1-(6-(3,5-dimethyl-1H-pyrazol-1-yl)-1,2,4,5-tetrazin-3-yl)piperidin-4-yl)-3-sulfamoylbenzamide (Ik)*. Yield, 65%. Red solid, mp 194–196 °C. ¹H NMR (400 MHz, DMSO-*d*₆) δ 8.18 (d, *J* = 7.3 Hz, 1H, H6), 7.75 (d, *J* = 3.6 Hz, 1H, H4), 7.53 (d, *J* = 4.9 Hz, 1H, H3), 7.07 (t, *J* = 4.3 Hz, 1H, NH), 6.13 (s, 1H, H4'), 4.84 (d, *J* = 13.6 Hz, 2H, N-CH₂-pip), 4.30–4.23 (m, 1H, N-CH-pip), 3.37 (t, *J* = 11.8 Hz, 2H, N-CH₂-pip), 2.52 (s, 3H, CH₃), 2.31 (s, 3H, CH₃), 2.13 (d, *J* = 12.8 Hz, 2H, -CH₂-pip), 1.74 (d, *J* = 14.1 Hz, 2H, -CH₂-pip). ¹³C NMR (101 MHz,

DMSO-*d*₆) δ 161.39 (C=O), 160.31 (C4''), 156.54 (C1''), 151.29 (C5'), 141.73 (C3 + C3'), 140.21 (C4), 130.15 (C1 + C2), 128.26 (C5), 127.54 (C6), 109.31 (C4'), 46.87 (C4''), 42.97 (C2''' + C6'''), 31.19 (C3''' + C5'''), 13.74 (CH₃), 13.17 (CH₃). IR (KBr, cm⁻¹): 2954, 1375, 1541, 1488, 1241. HRMS for (C₁₉H₂₃ClN₉O₃S [M + H]⁺). Calcd: 492.1333. Found: 492.1791.

4.2.2.12. *4-(Chloromethyl)-N-(1-(6-(3,5-dimethyl-1H-pyrazol-1-yl)-1,2,4,5-tetrazin-3-yl)piperidin-4-yl)benzamide (Il)*. Yield, 43%. Red solid, mp 201–203 °C. ¹H NMR (400 MHz, CDCl₃) δ 7.79 (d, *J* = 8.2 Hz, 2H, H2 + H6), 7.47 (d, *J* = 8.2 Hz, 2H, H3 + H5), 6.22 (d, *J* = 7.7 Hz, 1H, NH), 6.12 (s, 1H, H4'), 4.94 (d, *J* = 13.8 Hz, 1H, N-CH₂-pip), 4.62 (s, 2H, CH₂), 4.45–4.38 (m, 1H, N-CH-pip), 3.42–3.30 (m, 2H, N-CH₂-pip), 2.58 (s, 3H, CH₃), 2.35 (s, 3H, CH₃), 2.28 (dd, *J* = 12.7, 2.6 Hz, 2H, -CH₂-pip), 1.63 (qd, *J* = 12.3, 4.2 Hz, 2H, -CH₂-pip). ¹³C NMR (101 MHz, CDCl₃) δ 166.42 (C=O), 160.30 (C4''), 156.73 (C1''), 152.10 (C5'), 141.94 (C3'), 141.05 (C4), 134.27 (C1), 128.76 (C3 + C5), 127.40 (C2 + C6), 109.64 (C4'), 47.20 (C-Cl), 45.32 (C4''), 42.95 (C2''' + C6'''), 31.72 (C3''' + C5'''), 13.69 (CH₃), 13.45 (CH₃). IR (KBr, cm⁻¹): 3279, 1645, 1541, 1485, 1238. HRMS for (C₂₀H₂₃ClN₈O [M + H]⁺). Calcd: 427.1756. Found: 427.4261.

4.2.3. General synthetic procedure of compounds 2a-j

A mixture of 3,6-bis(3,5-dimethyl-1H-pyrazol-1-yl)-1,2,4,5-tetrazine **6** (1.0 mmol), TEA (triethylamine) (3 mmol), and the respective arylpiperazine or arylpiperidine (1.5 mmol) in acetonitrile (5 mL) was stirred overnight at room temperature. Then, the mixture was evaporated under vacuum to dryness, and the products were separated by flash column chromatography on silica gel eluting with CH₂Cl₂/MeOH (15:1).



X = CH for **2e**, for the rest of compounds **2**, X = N.

4.2.3.1. *3-(3,5-Dimethyl-1H-pyrazol-1-yl)-6-(4-phenylpiperazin-1-yl)-1,2,4,5-tetrazine (2a)*. Yield, 80%. Red solid, mp 196–197 °C. ¹H NMR (400 MHz, CDCl₃) δ 7.32–7.16 (m, 2H, H3 and H5), 6.87 (m, 3H, 3H, H2, H4 and H6), 6.10 (s, 1H, H4'), 4.25–4.10 (m, 4H, 2 × CH₂-pip), 3.40–3.28 (m, 4H, 2 × CH₂-pip), 2.58 (s, 3H, CH₃), 2.35 (s, 3H, CH₃). ¹³C NMR (50 MHz, CDCl₃) δ 160.33 (C4''), 156.79 (C1''), 152.01 (C5'), 150.77 (C1), 141.81 (C3'), 129.22 (C3 + C5), 120.66 (C4), 116.70 (C2 + C6), 109.57 (C4'), 49.11 (C3''' + C5'''), 43.55 (C2''' + C6'''), 13.64 (CH₃), 13.39 (CH₃). IR (KBr, cm⁻¹): 2921, 2820, 1611, 1561, 1240. HRMS for (C₁₇H₂₀N₈ [M + H]⁺). Calcd: 337.1884. Found: 337.1894.

4.2.3.2. *3-(3,5-Dimethyl-1H-pyrazol-1-yl)-6-(4-(4-nitrophenyl)piperazin-1-yl)-1,2,4,5-tetrazine (2b)*. Yield, 65%. Red solid, mp 199–201 °C. ¹H NMR (400 MHz, CDCl₃) δ 8.17 (d, *J* = 8.7 Hz, 2H, H3 + H5), 6.89 (d, *J* = 8.7 Hz, 2H, H2

+ H6), 6.11 (s, 1H, H4'), 4.30–4.08 (m, 4H, 2 × CH₂-pip), 3.72–3.50 (m, 4H, 2 × CH₂-pip), 2.58 (s, 3H, CH₃), 2.35 (s, 3H, CH₃). ¹³C NMR (101 MHz, CDCl₃) δ 160.38 (C4''), 157.11 (C1''), 154.30 (C5'), 152.37 (C1), 142.01 (C3'), 139.25 (C4), 125.98 (C3 + C5), 113.08 (C2 + C6), 109.91 (C4'), 46.54 (C3''' + C5'''), 43.00 (C2''' + C6'''), 13.71 (CH₃), 13.55 (CH₃). IR (KBr, cm⁻¹): 2983, 2850, 1597, 1484, 1321, 1240. HRMS for (C₁₇H₁₉N₉O₂ [M + H]⁺). Calcd: 382.1734. Found: 382.1750.

4.2.3.3. 3-(4-(4-Chlorophenyl)piperazin-1-yl)-6-(3,5-dimethyl-1H-pyrazol-1-yl)-1,2,4,5-tetrazine (**2c**). Yield, 69%. Red solid, mp 186–188 °C. ¹H NMR (400 MHz, CDCl₃) δ 7.21 (d, *J* = 8.9 Hz, 2H, H3 + H5), 6.87 (d, *J* = 8.9 Hz, 2H, H2 + H6), 6.08 (s, 1H, H4'), 4.24–4.08 (m, 4H, 2 × CH₂-pip), 3.37–3.20 (m, 4H, 2 × CH₂-pip), 2.54 (s, 3H, CH₃), 2.32 (s, 3H, CH₃). ¹³C NMR (101 MHz, CDCl₃) δ 160.28 (C4''), 156.79 (C1''), 152.01 (C5'), 149.34 (C1), 141.78 (C3'), 129.03 (C3 + C5), 125.45 (C4), 117.83 (C2 + C6), 109.60 (C4'), 49.00 (C3''' + C5'''), 43.36 (C2''' + C6'''), 13.61 (CH₃), 13.38 (CH₃). IR (KBr, cm⁻¹): 2960, 2820, 1553, 1280, 1240. HRMS for (C₁₇H₁₉ClN₈ [M + H]⁺). Calcd: 371.1494. Found: 371.1508.

4.2.3.4. 3-(3,5-Dimethyl-1H-pyrazol-1-yl)-6-(4-(4-methoxyphenyl)piperazin-1-yl)-1,2,4,5-tetrazine (**2d**). Yield, 71%. Red solid, mp 147–149 °C. ¹H NMR (400 MHz, CDCl₃) δ 7.01–6.90 (m, 2H, H3 + H5), 6.91–6.79 (m, 2H, H2 + H6), 6.08 (s, 1H, H4'), 4.24–4.11 (m, 4H, 2 × CH₂-pip), 3.76 (s, 3H, OCH₃), 3.26–3.12 (m, 4H, 2 × CH₂-pip), 2.55 (s, 3H, CH₃), 2.33 (s, 3H, CH₃). ¹³C NMR (101 MHz, CDCl₃) δ 160.30 (C4''), 156.74 (C1''), 154.47 (C4), 151.96 (C5'), 145.03 (C1), 141.78 (C3'), 118.98 (C2 + C6), 114.47 (C3 + C5), 109.53 (C4'), 55.43 (OCH₃), 50.62 (C3''' + C5'''), 43.69 (C2''' + C6'''), 13.62 (CH₃), 13.37 (CH₃). IR (KBr, cm⁻¹): 2910, 2820, 1513, 1240. HRMS for (C₁₈H₂₂N₈O [M + H]⁺). Calcd: 367.1989. Found: 367.2003.

4.2.3.5. 3-(3,5-Dimethyl-1H-pyrazol-1-yl)-6-(4-phenylpiperidin-1-yl)-1,2,4,5-tetrazine (**2e**). Yield, 84%. Red solid, mp 143–145 °C. ¹H NMR (400 MHz, CDCl₃) δ 7.39–7.14 (m, 5H, H2, H3, H4, H5, H6), 6.08 (s, 1H, H4'), 3.31–3.12 (m, 2H, CH₂-pip), 3.00–2.80 (m, 2H, CH₂-pip), 2.56 (s, 3H, CH₃), 2.34 (s, 3H, CH₃), 2.01–2.09 (m, 1H, CH), 1.95–1.64 (m, 4H, 2 × CH₂). ¹³C NMR (101 MHz, CDCl₃) δ 160.23 (C4''), 156.55 (C1''), 151.87 (C5'), 144.89 (C1), 141.76 (C3'), 128.60 (C3 + C5), 126.67 (C2 + C6), 126.59 (C4), 109.40 (C4'), 44.44 (C2''' + C6'''), 42.54 (C4'''), 32.75 (C3''' + C5'''), 13.67 (CH₃), 13.35 (CH₃). IR (KBr, cm⁻¹): 2923, 2853, 1577, 1486, 1247. HRMS for (C₁₈H₂₁N₇ [M + 2H]²⁺). Calcd: 337.1931. Found: 337.1894.

4.2.3.6. 3-(3,5-Dimethyl-1H-pyrazol-1-yl)-6-(4-(pyridin-2-yl)piperazin-1-yl)-1,2,4,5-tetrazine (**2f**). Yield, 65%. Red solid, mp 158–160 °C. ¹H NMR (400 MHz, CDCl₃) δ 8.20 (d, *J* = 4.7 Hz, 1H, H3), 7.51 (t, *J* = 7.8 Hz, 1H, H5), 6.68 (m, 2H, H4 + H6), 6.07 (s, 1H, H4'), 4.24–4.04 (m, 4H, 2 × CH₂-pip), 3.85–3.67 (m, 4H, 2 × CH₂-pip), 2.54 (s, 3H, CH₃), 2.32 (s, 3H, CH₃). ¹³C NMR (101 MHz, CDCl₃) δ 160.38 (C4''), 158.80 (C1), 156.78 (C1''), 151.99 (C5'), 147.91 (C3), 141.81 (C3'), 137.68 (C5), 113.97 (C4), 109.57 (C4'), 107.21 (C6), 44.66 (C3''' + C5'''), 43.26 (C2''' + C6'''), 13.63

(CH₃), 13.38 (CH₃). IR (KBr, cm⁻¹): 2920, 2850, 1490, 1238. HRMS for (C₁₆H₁₉N₉ [M + H]⁺). Calcd: 338.1836. Found: 338.1844.

4.2.3.7. 3-(3,5-Dimethyl-1H-pyrazol-1-yl)-6-(4-(pyridin-4-yl)piperazin-1-yl)-1,2,4,5-tetrazine (**2g**). Yield, 60%. Red solid, mp 183–185 °C. ¹H NMR (400 MHz, CDCl₃) δ 8.33 (d, *J* = 5.9 Hz, 2H, H3 + H5), 6.76 (d, *J* = 6.1 Hz, 2H, H2 + H6), 6.11 (s, 1H, H4'), 4.27–4.12 (m, 4H, 2 × CH₂-pip), 3.67–3.55 (m, 4H, 2 × CH₂-pip), 2.57 (s, 3H, CH₃), 2.35 (s, 3H, CH₃). ¹³C NMR (101 MHz, CDCl₃) δ 160.38 (C4''), 157.10 (C1''), 154.83 (C1), 152.36 (C5'), 149.12 (C3 + C5), 142.01 (C3'), 109.90 (C4'), 108.43 (C2 + C6), 45.45 (C3''' + C5'''), 42.91 (C2''' + C6'''), 13.71 (CH₃), 13.56 (CH₃). IR (KBr, cm⁻¹): 2924, 2854, 1611, 1550, 1241. ¹HRMS for (C₁₆H₁₉N₉ [M + H]⁺). Calcd: 338.1836. Found: 338.1847.

4.2.3.8. 3-(3,5-Dimethyl-1H-pyrazol-1-yl)-6-(4-(5-(trifluoromethyl)pyridin-2-yl)piperazin-1-yl)-1,2,4,5-tetrazine (**2h**). Yield, 60%. Red solid, mp 183–185 °C. ¹H NMR (400 MHz, CDCl₃) δ 8.43 (s, 1H, H6), 7.68 (d, *J* = 8.9 Hz, 1H, H4), 6.71 (d, *J* = 8.8 Hz, 1H, H3), 6.09 (s, 1H, H4'), 4.26–4.04 (m, 4H, 2 × CH₂-pip), 3.96–3.80 (m, 4H, 2 × CH₂-pip), 2.56 (s, 3H, CH₃), 2.56 (s, 3H, CH₃). ¹³C NMR (101 MHz, CDCl₃) δ 160.44 (C4''), 159.92 (C1), 156.96 (C1''), 152.20 (C5'), 145.74 (q, *J*_{CF} = 4.2 Hz, C3), 141.92 (C3'), 134.77 (q, *J*_{CF} = 2.9 Hz, C5), 124.37 (q, *J*_{CF} = 270.4 Hz, CF₃), 116.00 (q, *J*_{CF} = 33.1 Hz, C4), 109.75 (C4'), 105.72 (C6), 44.05 (C3''' + C5'''), 43.15 (C2''' + C6'''), 13.67 (CH₃), 13.47 (CH₃). ¹⁹F NMR (376 MHz, CDCl₃) δ -61.24. IR (KBr, cm⁻¹): 2923, 2854, 1611, 1277, 1241, 1082, 804. HRMS for (C₁₇H₁₈F₃N₉ [M + H]⁺). Calcd: 406.1710. Found: 406.1720.

4.2.3.9. 3-(3,5-Dimethyl-1H-pyrazol-1-yl)-6-(4-(pyrazin-2-yl)piperazin-1-yl)-1,2,4,5-tetrazine (**2i**). Yield, 59%. Red solid, mp 139–140 °C. ¹H NMR (400 MHz, CDCl₃) δ 8.20 (d, 1H, *J* = 1.4 Hz, H6), 8.10 (dd, 1H, *J* = 2.5, 1.6 Hz, H5), 7.92 (d, 1H, *J* = 2.6 Hz, H3), 6.09 (s, 1H, H4'), 4.16 (dd, *J* = 6.4, 4.2 Hz, 4H, 2 × CH₂-pip), 3.81 (dd, *J* = 6.4, 4.3 Hz, 4H, 2 × CH₂-pip), 2.56 (s, 3H, CH₃), 2.33 (s, 3H, CH₃). ¹³C NMR (50 MHz, CDCl₃) δ 160.45 (C4''), 156.95 (C1''), 154.54 (C1), 152.19 (C5'), 141.92 (C3'), 141.77 (C3), 133.78 (C4), 131.01 (C6), 109.74 (C4'), 43.94 (C3''' + C5'''), 43.12 (C2''' + C6'''), 13.66 (CH₃), 13.47 (CH₃). IR (KBr, cm⁻¹): 2922, 2853, 1488. HRMS for (C₁₅H₁₈N₁₀ [M + H]⁺). Calcd: 339.1789. Found: 339.1890.

4.2.3.10. 3-(3,5-Dimethyl-1H-pyrazol-1-yl)-6-(4-(5-nitropyridin-2-yl)piperazin-1-yl)-1,2,4,5-tetrazine (**2j**). Yield, 52%. Red solid, mp 201–203 °C. ¹H NMR (400 MHz, CDCl₃) δ 8.21 (d, 1H, *J* = 1.1 Hz, H6), 8.17–8.08 (m, 1H, H4), 7.93 (d, *J* = 2.6 Hz, 1H, H3), 6.09 (s, 1H, H4'), 4.26–4.09 (m, 4H, 2 × CH₂-pip), 3.92–3.75 (m, 4H, 2 × CH₂-pip), 2.56 (s, 3H, CH₃), 2.34 (s, 3H, CH₃). ¹³C NMR (101 MHz, CDCl₃) δ 160.46 (C4''), 156.96 (C1''), 154.55 (C1), 152.22 (C5'), 144.39 (C4), 141.93 (C3'), 133.90 (C3), 133.80 (C5), 131.04 (C6), 109.76 (C4'), 43.96 (C3''' + C5'''), 43.13 (C2''' + C6'''), 13.68 (CH₃), 13.49 (CH₃). IR (KBr, cm⁻¹): 2922, 2850, 1595, 1329, 1257, 1244. HRMS for (C₁₆H₁₈N₁₀O₂ [M + H]⁺). Calcd: 383.1687. Found: 383.1698.

4.2.4. Anticancer activity

Cancer cell lines were grown at 37 °C in humidified atmosphere and 5% CO₂. H1975, HL60, HCT116 and Vero cells were grown in RPMI 1640 culture medium supplemented with 10% foetal bovine serum and (100 UI/mL) penicillin-streptomycin. HeLa cells were grown in EMEM culture medium and supplemented with 10% foetal bovine serum and (100 UI/mL) penicillin-streptomycin.

4.2.4.1. Cytotoxicity study. Cytotoxicity assays were performed using the MTT reduction method as described in the literature (Faundez et al., 2005). Briefly, cancer cell lines were plated in a flat-bottom 96-wells plate at 1×10^4 cells per well density. Then, the cells were incubated with synthesized compounds at different concentrations (from 0.05 to 50 µM) in 200 µL of 10% foetal bovine serum-RPMI or EMEM culture medium at 37 °C for 72 h. 10 µL of MTT was added at a final concentration of 0.5 mg/mL, incubated at 37 °C for 4 h, and then solubilized with 10% sodium dodecyl sulphate (SDS) in 0.1 mM HCl and incubated overnight at 37 °C. Formazan formation was measured at 570 nm in a multiwell reader (StatFax 4200).

4.2.4.2. Viability assays with propidium iodide. Cell viability was analysed by FACS as previously described (Hetz et al., 2002; Villena et al., 2008; Aguirre et al., 2013). In this assay, after setting the baseline to exclude cell debris, cells impermeable to propidium iodide (PI negative) are considered as viable. Two populations of PI-permeable dead cells are distinguished based on fluorescence intensity, corresponding to either hypodiploid apoptotic cells or necrotic cells with intact DNA. Here, H1975, HCT116, and HeLa cells were incubated with concentrations of 50 µM of each compound for 16 h at 37 °C. Cells were harvested and stained with 10 µg/mL of propidium iodide to determine cell viability. Samples containing roughly 1×10^4 cells were evaluated by flow cytometry (FACScanto II; Becton Dickinson, Mountain View, CA) and analysed using the software program FCS Express v5.

4.2.4.3. Statistical analysis. Values are expressed as means \pm standard deviations from three independent experiments. IC₅₀ values (Compound concentration necessary to decrease at 50% the MTT reduction) and the two-way analysis of variance (ANOVA) test were performed when necessary with Prism GraphPad 6.0f software (GraphPad Software Inc.).

4.2.5. 3D-QSAR

4.2.5.1. Selection of conformers and molecular alignment. CoMFA and CoMSIA studies were performed with Sybyl X-1.2 software installed in a Windows 7 environment on a PC with an Intel core i7 CPU. In order to get the best conformers for each molecule, every compound was subjected to a preliminary geometry optimization of 1000 iterations using the Tripos force field implemented in Sybyl (Vinter et al., 1987). The convergence criterion of the energy gradient was set to 0.005 kcal/molÅ, and the Gasteiger-Hückel charges were assigned to each atom (Gasteiger and Marsili, 1980). Then, 20 cycles of simulated annealing dynamics were run, heating the molecules to 2000 K for 2000 fs followed by the annealing of the compounds at 0 K for 10,000 fs. Twenty minimal energy conformers for each compound were selected and a preliminary 3D-QSAR model was generated. From this analysis,

the best conformers for each compound were chosen for the definitive CoMFA and CoMSIA studies. The minimized structures were superimposed by the Distill alignment protocol as implemented in Sybyl.

4.2.5.2. External validation of the CoMFA and CoMSIA models. The predictive power of the models was assessed by the calculation of the predictive r^2 (r_{pred}^2) for both CoMFA and CoMSIA models. r_{pred}^2 , which measures the predictive performance of a PLS model, is defined according to Eq. (1):

$$r_{pred}^2 = 1 - \frac{\sum_{i=1}^n (y_i - x_i)^2}{\sum_{i=1}^n (x_i - \bar{x})^2} \quad (1)$$

where y_i is the predicted biological activity value of every molecule in the test set, x_i is the actual biological activity value of every molecule in the test set, and \bar{x} is the mean activity of the training set molecules.

4.2.5.3. CoMFA and CoMSIA field calculation. To derive CoMFA and CoMSIA descriptor fields, the aligned training set molecules were placed in a 3D cubic lattice with grid spacing of 2 Å in x , y , and z directions such that the entire set was included. CoMFA steric and electrostatic field energies were calculated using a sp^3 carbon probe atom with a Van der Waals radius of 1.52 Å and a charge of +1.0. Cut-off values for both steric and electrostatic fields were set to 30.0 kcal/mol. For CoMSIA analysis, standard settings [probe with charge +1.0, radius 1 Å, hydrophobicity +1.0, hydrogen-bond donating +1.0, hydrogen bond accepting +1.0] (Klebe et al., 1994) were used to calculate five different fields: steric, electrostatic, hydrophobic, acceptor and donor. Gaussian-type distance dependence was used to measure the relative attenuation of the field position of each atom in the lattice, and led to much smoother sampling of fields around the molecules when compared to CoMFA. The default value of 0.3 was set for attenuation factor α .

4.2.5.4. Partial Least Squares (PLS) analysis. PLS analysis was used to construct a linear correlation between the CoMFA/CoMSIA descriptors (independent variables) and the activity values (dependent variables) (Clark et al., 1989). To select the best model, cross-validation analysis was performed using the LOO method (and SAMPLS), which generates the square of the cross-validation coefficient (q^2) and the optimum number of components (N). Non-cross-validation was performed with a column filter value of 2.0 in order to speed up analysis and reduce noise.

Author contributions

A. Cañete-Molina, C. Espinosa-Bustos and M. González-Castro synthesized and characterized all compounds. C. Espinosa-Bustos and R.A. Tapia, analysed the data and help to write the paper. C. Espinosa-Bustos, A. Aguirre and M. Faúndez performed the biological assays. J. Mella performed the 3D-QSAR study. A.R. Cabrera and I. Brito, performed the crystallographic measurement and processed the data. C. O. Salas designed, analysed and supervised the research and wrote the paper. All authors read and approved the final manuscript.

Acknowledgements

Authors gratefully acknowledge financial support from FONDECYT (Research Grant) N° 1120128 and 1161816.

Appendix A. Supplementary material

Supplementary data associated with this article can be found, in the online version, at <http://dx.doi.org/10.1016/j.arabjc.2017.04.002>.

References

- Abou-Seri, S.M., Eldehna, W.M., Ali, M.M., Abou El Ella, D.A., 2016. *Eur. J. Med. Chem.* 107, 165.
- Abouzid, K.A.M., Khalil, N.A., Ahmed, E.M., 2012. *Med. Chem. Res.* 21, 3288.
- Aguirre, A., Shoji, K.F., Saez, J.C., Henriquez, M., Quest, A.F.G., 2013. *J. Cell. Physiol.* 228, 485.
- Banerjee, U., Hadden, M.K., 2014. *Expert Opin. Drug Discov.* 9, 751.
- Bender, M.H., Hipskind, P.A., Capen, A.R., Cockman, M., Credille, K.M., Gao, H., Bastian, J.A., Clay, J.M., Lobb, K.L., Sall, D.J., Thompson, M.L., Wilson, T., Wishart, G.N., Patel, B.K.R., 2011. *Cancer Res.* 71, 2819.
- Bold, G., Altmann, K.H., Frei, J., Lang, M., Manley, P.W., Traxler, P., Wietfeld, B., Bruggen, J., Buchdunger, E., Cozens, R., Ferrari, S., Furet, P., Hofmann, F., Martiny-Baron, G., Mestan, J., Rosel, J., Sills, M., Stover, D., Acemoglu, F., Boss, E., Emmenegger, R., Lasser, L., Masso, E., Roth, R., Schlachter, C., Vetterli, W., Wyss, D., Wood, J.M., 2000. *J. Med. Chem.* 43, 2310.
- Chan, E.L., Chin, C.H., Lui, V.W., 2016. *Future Oncol.* 12, 71.
- Clark, M., Cramer, R.D., Vanopdenbosch, N., 1989. *J. Comput. Chem.* 10, 982.
- Coburn, M.D., Buntain, G.A., Harris, B.W., Hiskey, M.A., Lee, K.-Y., Ott, D.G., 1991. *J. Heterocycl. Chem.* 28, 2049.
- Cramer, R.D., Patterson, D.E., Bunce, J.D., 1988. *J. Am. Chem. Soc.* 110, 5959.
- Devaraj, N.K., Weissleder, R., Hilderbrand, S.A., 2008. *Bioconjug. Chem.* 19, 2297.
- Devaraj, N.K., Weissleder, R., 2011. *Acc. Chem. Res.* 44, 816.
- Dolezal, M., Zitko, J., 2015. *Expert Opin. Ther. Pat.* 25, 33.
- Dörsam, B., Fahrner, J., 2016. *Cancer Lett.* 371, 12.
- Dragovich, T., Laheru, D., Dayyani, F., Bolejack, V., Smith, L., Seng, J., Burris, H., Rosen, P., Hidalgo, M., Ritch, P., Baker, A.F., Raghunand, N., Crowley, J., Von Hoff, D.D., 2014. *Cancer Chemother. Pharmacol.* 74, 379.
- Eldehna, W.M., Ibrahim, H.S., Abdel-Aziz, H.A., Farrag, N.N., Youssef, M.M., 2015. *Eur. J. Med. Chem.* 89, 549.
- Faundez, M., Pino, L., Letelier, P., Ortiz, C., Lopez, R., Seguel, C., Ferreira, J., Pavani, M., Morello, A., Maya, J.D., 2005. *Antimicrob. Agents Chemother.* 49, 126.
- Gasteiger, J., Marsili, M., 1980. *Tetrahedron* 36, 3219.
- Hetz, C.A., Hunn, M., Rojas, P., Torres, V., Leyton, L., Quest, A.F.G., 2002. *J. Cell. Sci.* 115, 4671.
- Khan, I., Ibrar, A., Abbas, N., 2014. *Arch. Pharm.* 347, 1.
- Klebe, G., Abraham, U., Mietzner, T., 1994. *J. Med. Chem.* 37, 4130.
- Lanning, M.E., Yu, W., Yap, J.L., Chauhan, J., Chen, L., Whiting, E., Pidugu, L.S., Atkinson, T., Bailey, H., Li, W., Roth, B.M., Hynicka, L., Chesko, K., Toth, E.A., Shapiro, P., MacKerell Jr., A.D., Wilder, P.T., Fletcher, S., 2016. *Eur. J. Med. Chem.* 113, 273.
- Liao, C., Sitzmann, M., Pugliese, A., Nicklaus, M.C., 2011. *Future Med. Chem.* 3, 1057.
- McBride, C., Cheruvallath, Z., Komandla, M., Tang, M., Farrell, P., Lawson, J.D., Vanderpool, D., Wu, Y., Dougan, D.R., Plonowski, A., Holub, C., Larson, C., 2016. *Bioorg. Med. Chem. Lett.* 26, 2779.
- Meanwell, N.A., 2011. *J. Med. Chem.* 54, 2529.
- Miller-Moslin, K., Peukert, S., Jain, R.K., McEwan, M.A., Karki, R., Llamas, L., Yusuff, N., He, F., Li, Y., Sun, Y., Dai, M., Perez, L., Michael, W., Sheng, T., Lei, H., Zhang, R., Williams, J., Bourret, A., Ramamurthy, A., Yuan, J., Guo, R., Matsumoto, M., Vattay, A., Maniara, W., Amaral, A., Dorsch, M., Kelleher 3rd, J.F., 2009. *J. Med. Chem.* 52, 3954.
- Moreira-Lima, L., Barreiro, E.J., 2005. *Curr. Med. Chem.* 12, 23.
- NCI, NCI/NIH Developmental Therapeutics Program, 2014.
- Ni, M., Esposito, E., Raj, V.P., Muzi, L., Zunino, F., Zuco, V., Cominetti, D., Penco, S., Dal Pozzo, A., 2015a. *Bioorg. Med. Chem.* 23, 6785.
- Ni, Z., Zhou, L., Li, X., Zhang, J., Dong, S., 2015b. *PLoS ONE* 10, e0141918.
- Patel, R.V., Park, S.W., 2013. *Mini-Rev. Med. Chem.* 13, 1579.
- Patra, S., Sarkar, B., Ghumaan, S., Fiedler, J., Kaim, W., Lahiri, G. K., 2004. *Inorg. Chem.* 43, 6108.
- Peukert, S., He, F., Dai, M., Zhang, R., Sun, Y., Miller-Moslin, K., McEwan, M., Lagu, B., Wang, K., Yusuff, N., Bourret, A., Ramamurthy, A., Maniara, W., Amaral, A., Vattay, A., Wang, A., Guo, R., Yuan, J., Green, J., Williams, J., Buonamici, S., Kelleher 3rd, J.F., Dorsch, M., 2013. *ChemMedChem* 8, 1261.
- Rani, R., Kumar, V., 2016. *J. Med. Chem.* 59, 487.
- Ruch, J.M., Kim, E.J., 2013. *Drugs* 73, 613.
- Rusinov, G.L., Latosh, N.I., Ganebnykh, I.I., Ishmetova, R.I., Ignatenko, N.K., Chupakhin, O.N., 2006. *Russ. J. Org. Chem.* 42, 757.
- Sheldrick, G.M., 2008. *Acta Crystallogr. A.* 64, 112.
- Sherer, C., Snape, T.J., 2015. *Eur. J. Med. Chem.* 97, 552.
- Shiro, T., Fukaya, T., Tobe, M., 2015. *Eur. J. Med. Chem.* 97, 397.
- Siegel, R., Naishadham, D., Jemal, A., 2013. *CA Cancer. J. Clin.* 63, 11.
- Stoe & Cie, 2001. X-Area and X-Red. Stoe&Cie, Darmstadt, Germany.
- Villena, J., Henriquez, M., Torres, V., Moraga, F., Diaz-Elizondo, J., Arredondo, C., Chiong, M., Olea-Azar, C., Stutzin, A., Lavandero, S., Quest, A.F.G., 2008. *Free Radical Bio. Med.* 44, 1146.
- Vinter, J.G., Davis, A., Saunders, M.R., 1987. *J. Comput. Aided Mol. Des.* 1, 31.
- Wang, Y., Cheng, F.X., Yuan, X.L., Tang, W.J., Shi, J.B., Liao, C.Z., Liu, X.H., 2016. *Eur. J. Med. Chem.* 112, 231.
- Wilson, T., Vetman, T., Sall, D.J., Bastian, J.A., Lobb, K.L., Clay, J. M., Zhang, B., Cohen, J.D., Bender, D.M., Bender, M.H., Capen, A.R., Perkins, E.J., Patel, B.K.R., Hipskind, P.A., 2013. *Abstr. Pap. Am. Chem. Soc.* 246.
- Wu, H., Yang, J., Seckute, J., Devaraj, N.K., 2014. *Angew. Chem. Int. Ed. Engl.* 53, 5805.
- Xin, M., 2015. *Expert Opin. Ther. Pat.* 25, 549.
- Xu, F., Yang, Z., Jiang, J., Pan, W., Yang, W., Wu, J., Zhu, Y., Wang, J., Shou, Q., Wu, H., 2016. *Bioorg. Med. Chem. Lett.* 26, 3042.
- Zhang, S.L., Zhao, Y.F., Liu, Y.J., Chen, D., Lan, W.H., Zhao, Q.L., Dong, C.C., Xia, L., Gong, P., 2010. *Eur. J. Med. Chem.* 45, 3504.